Maiasaura, a model organism for extinct vertebrate population biology: a large sample statistical assessment of growth dynamics and survivorship

Holly N. Woodward, Elizabeth A. Freedman Fowler, James O. Farlow, and John R. Horner

Abstract.—Fossil bone microanalyses reveal the ontogenetic histories of extinct tetrapods, but incomplete fossil records often result in small sample sets lacking statistical strength. In contrast, a histological sample of 50 tibiae of the hadrosaurid dinosaur *Maiasaura peeblesorum* allows predictions of annual growth and ecological interpretations based on more histologic data than any previous large sample study. Tibia length correlates well ($R^2 > 0.9$) with diaphyseal circumference, cortical area, and bone wall thickness, thereby allowing longitudinal predictions of annual body size increases based on growth mark circumference measurements. With an avian level apposition rate of 86.4 μm/day, *Maiasaura* achieved over half of asymptotic tibia diaphyseal circumference within its first year. Mortality rate for the first year was 89.9% but a seven year period of peak performance followed, when survivorship (mean mortality rate = 12.7%) was highest. During the third year of life, *Maiasaura* attained 36% (x = 1260 kg) of asymptotic body mass, growth rate was decelerating (18.2 μm/day), cortical vascular orientation changed, and mortality rate briefly increased. These transitions may indicate onset of sexual maturity and corresponding reallocation of resources to reproduction. Skeletal maturity and senescence occurred after 8 years, at which point the mean mortality rate increased to 44.4%. Compared with *Alligator*, an extant relative, *Maiasaura* exhibits rapid cortical increase early in ontogeny, while *Alligator* cortical growth is much lower and protracted throughout ontogeny. Our life history synthesis of *Maiasaura* utilizes the largest histological sample size for any extinct tetrapod species thus far, demonstrating how large sample microanalyses strengthen paleobiological interpretations.

Holly N. Woodward*. Museum of the Rockies, 600 West Kagy Boulevard, Bozeman, Montana 59717, U.S.A. E-mail: holly.n.woodward@gmail.com. *Present address: Department of Anatomy and Cell Biology, Oklahoma State University Center for Health Sciences, 1111 West 17th Street, Tulsa, Oklahoma 74107, U.S.A.

Elizabeth A. Freedman Fowler and John R. Horner. Montana State University, Museum of the Rockies and Department of Earth Sciences, 600 West Kagy Boulevard, Bozeman, Montana 59717, U.S.A.

James O. Farlow. Indiana Purdue University, Department of Geosciences, 2101 Coliseum Boulevard East, Fort Wayne, Indiana 46805, U.S.A.

Introduction

Vertebrate bone tissue microstructures reveal ontogenetic status, physiology, annual growth rate, and sexual maturity (Cormack 1987; Francillon-Vieillot et al. 1990; Games 1990; de Margerie et al. 2004; Schweitzer et al. 2005; Montes et al. 2010), thereby permitting life history reconstructions of animals long extinct. Such analyses are applied to fossils of non avian dinosaurs, but small sample sizes can lead to inaccurate life history summaries. A laterally extensive monodominant bonebed, yielding thousands of fossils from the hadrosaurid dinosaur *Maiasaura peeblesorum*, offers a unique opportunity for large scale histologic

analysis of an extinct taxon. Here we present a comprehensive growth series analysis of *Maiasaura peeblesorum*. Our study is different from other large scale paleohistology studies because it represents the largest single element, single taxon, and single population osteohistology synthesis to date for an extinct tetrapod. Additionally, every skeletal element sampled preserves the entire growth mark record, so that no retrocalculations for age determination were required for any specimen in our study. We hypothesize that our ontogenetic sample size of 50 histologically examined tibiae will permit more meaningful interpretations of ontogenetic growth, individual variation, and population biology, while allowing us to test

established extinct tetrapod osteohistology hypotheses and assumptions that are based on less data.

Fossil remains of *Maiasaura* from a nesting horizon (Museum of the Rockies locality TM-160) in the Campanian Two Medicine Formation of Montana initially attracted scientific attention by providing the first evidence that at least some dinosaur taxa nested in colonies and that the altricial hatchlings were cared for by adults (Horner and Makela 1979; Barreto 1997; Horner et al. 2001). In the years that followed, *Maiasaura* specimens collected from a bonebed (Museum of the Rockies localities TM-003, TM-151, TM-158) overlying the nesting horizon revealed an ontogenetic shift from bipedality to quadrupedality (Dilkes 2000, 2001), intraskeletal variation in bone apposition rates, and maximum growth rates similar to those observed in extant large bodied mammals and birds (Horner et al. 2000).

For the present study, samples of 50 *Maiasaura* tibiae were histologically examined to assess individual variation in growth and to produce the largest sample set to date for a dinosaur population biology synthesis. The tibia sample derives from decades of collecting from the *Maiasaura* bonebed, which spans at least two square kilometers and contains thousands of disarticulated *Maiasaura* skeletal elements (Varricchio and Horner 1993) with very little time averaging (Trueman and Benton 1997). The tibia sample encompasses early juveniles (~3.0 m in body length) to skeletally mature adults (>7 m in body length) (Horner et al. 2000). No perinatal material is present in the bonebed, so to construct a complete ontogenetic growth history we include a perinatal tibia from the nesting horizon for hatchling measurements.

The level of analysis provided by this large sample size allows more statistical strength in calculations of annual growth than previous large scale studies, and is based on the bone tissue of individual tibiae without requiring retrocalculations to account for any missing years of growth. Such a sample reveals ontogenetic patterns and individual variation easily overlooked with smaller sample sets. The statistical power provided by a sample of 50 tibiae (Steinsaltz and Orzack 2011) also permits more meaningful hypotheses of dinosaur survivorship curves. Our life history synthesis incorporates and builds upon previous *Maiasaura* studies (Horner and Makela 1979; Horner 1982, 1983; Varricchio and Horner 1993; Barreto 1997; Horner 1999; Dilkes 2000; Horner et al. 2000; Dilkes 2001; Horner et al. 2001) and with the addition of the data acquired here, *Maiasaura* becomes the most ontogenetically well understood dinosaur species, allowing the most thorough evaluation of the life history of any extinct tetrapod thus far.

Institutional Abbreviations.—MOR, Museum of the Rockies; ROM, Royal Ontario Museum; YPM-PU, Princeton University collections now curated at the Yale Peabody Museum.

Materials and Methods

Maiasaura peeblesorum skeletal elements, including the tibiae used in this study, were collected over a period of more than thirty years from three bonebed localities (MOR localities TM-003, TM-151, TM-158) within the Two Medicine Formation in an area of badland exposures approximately 19 km west of Choteau, Montana. The TM-003 locality is approximately 153 m northwest of TM-158, and approximately 629 m southeast of TM-151. Although erosion along the Willow Creek anticline geographically separates the sites, a bentonite layer is present approximately 4.3 m above all three localities (Lorenz and Gavin 1984; Varricchio et al. 2010) and the sites are stratigraphically correlated (Schmitt et al. 2014), representing a single 0.4–1.5 m thick bonebed, laterally traceable for approximately 2 km (Schmitt et al. 2014). The bentonite layer is dated to 75.92 ± 0.32 Ma (using the standard of MMhb-1 = 523.1 Ma) (Varricchio et al. 2010). The presence of red beds, caliche horizons, and grey to red mudstones suggests that the Two Medicine Formation was deposited during semi arid conditions that included a long dry season and warm temperatures (Lorenz and Gavin 1984).

Hadrosaur bones dominate the bonebed, and *Maiasaura peeblesorum* is the only hadrosaurid taxon identified to the species level; there is no evidence of a second hadrosaurid taxon being present. A study by Schmitt et al. (2014)

examined 189 previously excavated bones from various localities in the bonebed as well as 58 bones recovered from a 2 m² test pit near TM-003. From the 247 skeletal elements examined, 171 (69.2%) are referred to Hadrosauridae, 15 (6.1%) to Maiasaurinae (sensu Horner 1992, currently Brachylophosaurini sensu Gates et al. 2011), and seven (2.8%) assigned to *Maiasaura peeblesorum*. The sample also included five theropod (2%) and 49 (19.8%) unidentified skeletal elements (Schmitt et al. 2014). Fossils referred to as *Maiasaura* collected from these bonebed localities include unassociated cranial, axial, and appendicular skeletal elements.

The bonebed was most likely the result of a sediment gravity flow that varied temporally and spatially between a non cohesive debris flow and a hyperconcentrated flow (Schmitt et al. 2014). A small component of the bonebed assemblage is likely made of bone incorporated from shallow scouring (10–30 cm in depth) of the underlying floodplain deposit substrate. Modern rates of floodplain sediment accumulation suggest a minimum of 10^{-2} years of time averaging for the exhumed skeletal elements (Schmitt et al. 2014). Based on a lack of significant weathering features, the majority of hadrosaurid bones in the bonebed represent a minimal surface residence time of 0.1–10 years (Rogers 1993; Schmitt et al. 2014). Geochemical analyses (Trueman 1999) also suggest this is a transported, weakly time averaged assemblage.

Ecological interpretation of tibia age frequency distribution, consisting largely of the very young and fewer adults or near adult animals (Fig. 1), is neither strongly attritional nor catastrophic. This is because the sample size of non juveniles is low enough that the abundances are not statistically significant, which could mask a catastrophic age profile. However, as was also suggested in Schmitt et al. (2014), we interpret the nearly monodominant nature of the bonebed, its fossil density, and weak time averaging as representing one or more transported catastrophic death episodes possibly related to drought or disease (Rogers 1990; Varricchio and Horner 1993; Schmitt et al. 2014)
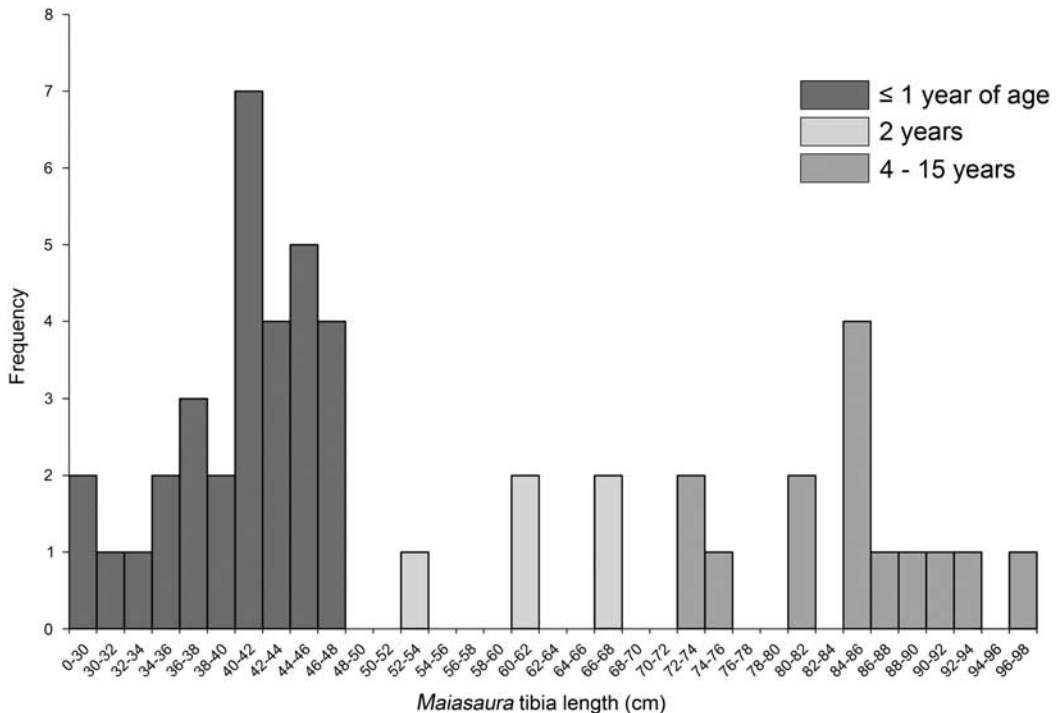

FIGURE 1.   Histogram of measured *Maiasaura* tibia lengths and corresponding ages obtained from growth mark counts. Over half of the tibiae in the sample were from individuals less than one year of age. Of the remaining 19 tibiae, five were from individuals two years of age; three year olds were absent; and the rest were from individuals between four and 15 years of age (n = 50).

that selectively targeted weaker animals. Of any age grouping, those within their period of "peak performance" (i.e., when survival and reproductive rates are highest (Jones et al. 2008; Nussey et al. 2008; Nussey et al. 2009)) were most likely to survive the events, and are therefore not strongly represented within the assemblage. Thus, even if the cause of death was catastrophic, it could have been age selective, producing an age profile more similar to an attritional assemblage. Regardless of cause of death, due to low time averaging, we consider this bonebed to represent a population of *Maiasaura* that experienced similar seasonal environmental stresses over a geologically brief period of time, so that observed differences in bone microstructure should be influenced largely by individual genetic variability in growth and less so by environmental differences.

From the fossils collected, 50 of the most complete tibiae (MOR 005 and MOR 758) were used in this study. Due to several factors, it is highly unlikely that any two contralateral tibiae included in our study were from the same individual. Such factors include: the density of *Maiasaura* fossils in the bonebed; the completely disarticulated nature of all the elements documented; the lateral extent of the bonebed; and the geographically (but not stratigraphically) separate sites within the bonebed from which specimens were collected. Therefore we report that the tibia sample set represents a minimum of 32 individuals (based on number of right tibiae) to set a lower limit on the number of individuals included in this study, but we will for the purposes of this paper consider each of the 50 tibiae to represent a single individual.

To make the results of bone microstructure analyses comparable across studies, researchers often select the femur for sectioning. But as with all hadrosaurids, the fourth trochanter in the femur of *Maiasaura* extends to nearly half the length of the diaphysis. This bony process is remodeled frequently during growth, thus affecting the visibility of primary tissue along most of the diaphyseal length. The tibia was chosen for analysis because it lacks such a process and is therefore less subject to extensive remodeling. Although there is variation in the apposition rates of different bones within a

skeleton (Horner et al. 1999; Cullen et al. 2014; Woodward et al. 2014), this study samples only tibiae in order to directly compare variability present in a single element across multiple individuals. Along with the femur, the tibia tends to provide the most consistent skeletochronological results (Horner et al. 1999), allowing reasonable estimates of maximum growth rates.

Tibiae collected from the bonebed and used in this project were numbered T1 through T50. Each was photographed and hand traced in lateral view prior to thin sectioning. The straight line distance from the anterior edge of the cnemial crest to the distal tip of the lateral malleolus was recorded (n = 35) and conservative length estimates were made (Supplementary Table 1) in cases where either epiphysis was incomplete (n = 13). Only three tibiae (T34, T49, T50) within the sample were too incomplete for reasonable length estimates.

A section of the diaphysis containing the least circumference (location determined by using a fabric tape measure) for each tibia was removed using a wet tile saw fitted with a continuous rim diamond blade, and then prepared following Lamm (2013). The location of the least diaphyseal circumference was found to vary between 36.5% and 61.4% (x = 48.8%) the length of the tibia as measured from the end of the lateral malleolus, regardless of ontogenetic status (Supplementary Fig. 1). Two transverse sections from the tibial shaft, each approximately 0.3 cm in thickness, were removed to either side of the line of minimum diaphyseal circumference. In most cases, only one of the two slices was completely processed for analysis while the second was held as a duplicate.

Completed slides were examined at either 10× or 40× total magnifications using a Nikon Optiphot-Pol polarizing microscope. Photomicrographs of the entire sections were taken incrementally using a Nikon DS-Fi1 digital sight camera, and compiled using NIS-Elements BR 3.0 software to create a single image from multiple photographs. Thus, these composite images often have a mosaic appearance. Transverse section periosteal surface circumferences as well as circumferences of medullary cavities and lines of arrested growth (LAGs) were traced in Adobe Photoshop CS3. Qualitative descriptions of bone tissue

organization and vascular canal orientation apply the terminology from Francillon-Vieillot et al. (1990). Lines of arrested growth were identified as narrow (approximately between 10 and 30 μm thickness) black rings encircling the cortex, separating bone laminae on either side. In extant vertebrates, a LAG is a hypermineralized tissue representing the periosteal surface during temporarily arrested growth, and having an annual periodicity in extant vertebrates for which data exist (Peabody 1961; Castanet et al. 1993; Köhler et al. 2012). Therefore, we assume the same cause and periodicity holds true for LAGs found in *Maiasaura*. The LAGs in *Maiasaura* tibiae never cross cut bone laminae but followed them, and passed around vascular canals rather than through them. Unless obfuscated by diagenetic crushing, periosteal surface erosion, or secondary reconstruction, cortical LAGs could be fully traced. Only within the closely spaced LAGs representing the external fundamental system (EFS) of skeletally mature adults (Cormack 1987; Castanet et al. 1988) were growth marks difficult to fully trace due to their close spacing, splitting, or merging.

Another way in which the *Maiasaura* sample set is unique is that each specimen contains a complete LAG record. This is true in even the largest, skeletally mature specimens that are not diagenetically altered. In the large specimens, secondary remodeling and medullary expansion only partially obliterate the innermost LAG. The circumference of this partial innermost LAG corresponds with the shape and circumference of the largest tibiae for which no LAGs are present (i.e., juveniles dying just prior to the close of their first year of growth). This test therefore confirms that a full LAG record is preserved in large tibiae and makes the need for retrocalculations of missing LAGs unnecessary.

Periosteal and LAG circumferences, as well as the total area of the transverse section enclosed by the circumferences (here termed cortical area), were quantified using NIH ImageJ (Rasband 1997–2014) and the BoneJ plugin (Doube et al. 2010) (Supplementary Table 1; Supplementary Table 2). High resolution versions of images discussed in this manuscript are accessible on MorphoBank (www.morphobank.org), project number P1139. Images of full transverse sections of three tibiae are also accessible in the same MorphoBank project. These include T16 (Morphobank image M326121), with no LAGs; T31 (M340003), with two LAGs; and T46 (M340007), with nine LAGs in the cortex and four in the EFS.

Individual average cortical apposition rates were calculated (Table 1) for each year of growth by using tibiae possessing LAGs as well as complete, uncrushed transverse diaphyseal sections (n = 9). The distances along major and minor axes from the geometric centroid to the first LAG were measured and averaged to obtain a cortical thickness

TABLE 1. Changes in *Maiasaura* bone tissue apposition rate based on zonal bone thickness. Rates are measured in micrometers per day. The "Conventional apposition rate" reports the daily apposition rate of bone if it were deposited continuously throughout a 365-day year, and is the method used in previous dinosaur cortical apposition rate studies. The "90-day hiatus" represents the daily apposition rate of bone deposited continuously throughout the growth season, with zero apposition during an estimated 90-day unfavorable season. "Increasing hiatus" instead assumes a constant apposition rate of 84.8 μm/day during 365 days of the first year, then maintaining the same rate during the growing season but with an increasing hiatus duration each year, determined by average cortical zone thickness.

	n	Conventional apposition rate		90 day growth hiatus		Increasing hiatus and constant apposition	
		Mean apposition rate (micrometers/day)	Standard deviation	Mean apposition rate (micrometers/day)	Standard deviation	Mean growing days	Standard deviation
LAG1	9	65.1	5.9	86.4	7.9	365	0.0
LAG2	9	21.4	6.2	28.4	8.2	120	35.3
LAG3	5	13.7	2.1	18.2	2.8	73	10.0
LAG4	4	6.9	2.8	9.2	3.7	39	17.0
LAG5	4	5.9	2.1	7.8	2.8	32	13.0
LAG6	3	2.9	1.7	3.9	2.3	17	9.8
LAG7	2	5.8	0.1	7.6	0.1	33	0.5
LAG8	1	2.4	0.0	3.2	0.0	14	0.0
LAG9	1	2.6	0.0	3.5	0.0	15	0.0

(Supplementary Table 3). This procedure was repeated for each consecutive LAG so that average annual apposition for each individual could be determined. Annual apposition was then converted to a daily rate (µm/day) based on a 365 day year, to allow direct comparisons with extant taxa (Myhrvold 2013). Maximum average daily apposition rates were also calculated (Table 1), assuming a three month (90 day) growth hiatus as determined for extant bovids (Köhler et al. 2012). As an alternative, yearly increase of growth hiatus duration was calculated (Table 1) assuming that apposition rate is constant throughout ontogeny and that it is the growth hiatus that increases as individuals age. For each scenario, apposition rates of cortical thickness between the outermost LAG and the periosteal surface were not calculated as this thickness does not represent a single year of growth (either less than a year in growing animals, or many years if the external fundamental system is present).

Survivorship curves were previously modeled for *Albertosaurus, Daspletosaurus, Tyrannosaurus,* and *Psittacosaurus* (Erickson et al. 2006; Erickson et al. 2009; Erickson et al. 2010), but our study is the first to model extinct tetrapod survivorship using a sample size with more than 30 specimens for which age has been histologically determined for each. The 95% confidence intervals for the survivorship curve were calculated using the method of Steinsaltz and Orzack (2011): of N individuals in the sample, k individuals survive x years, so the 95% confidence interval for each year is calculated using the formula $k/N \pm 1.96\sqrt{k(N-k)/N^3}$. Mean annual mortality rates over specific age ranges were also calculated using the method of Steinsaltz and Orzack (2011: Table 2). Within an age range, the number of deaths d is divided by E, "the total number of years lived by all individuals until d deaths occur," (Steinsaltz and Orzack 2011: p. 116) to yield the mean annual mortality rate $\hat{\mu} = d/E$. The ratio of mortality rates in one age range to another has the F distribution, with degrees of freedom $2d_1$ and $2d_2$ (two times the number of deaths in each age range). The two tailed 95% confidence interval for the F distribution, given those degrees of freedom, is then multiplied by the mortality ratio to yield the 95% confidence

interval for the mortality ratio. If the confidence interval does not include 1.0, then the mean annual mortality rates for the two age ranges are significantly different at $\alpha = 0.05$. The combination of age ranges with the smallest 95% confidence interval also represents the age ranges with the greatest difference in mortality rates; this was used to divide the *Maiasaura* sample into three age groups with different mortality rates. Because the degree of neonate mortality is unknown (or at least not recorded in the TM-003, TM-151, and TM-158 localities), the mean annual mortality for the juvenile age range is a minimum estimate.

The R^2 values of regressions were determined in Microsoft Office Excel 2003 for the relationship between tibia length and: minimum diaphyseal circumference, total transverse section cortical area, medullary cavity area, medullary cavity circumference, and bone wall thickness (i.e., the area of the transverse section excluding the medullary cavity) (Supplementary Tables 4–8). In several specimens the periosteal surface was largely missing or crushed (n = 6), the tibia length was too incomplete to obtain accurate measurements (n = 2), or circumference measurements were not obtained (n = 2). Therefore, out of the 50 tibiae, only 40 were used to construct diaphyseal circumference regressions and transverse section area regressions. Medullary cavity area, medullary cavity circumference, and bone wall thickness regressions were determined from the 29 specimens from which both diaphyseal area and medullary cavity measurements were recorded.

From the tibia length and LAG circumference measurements, *Maiasaura* annual ontogenetic growth can be illustrated in a linear dimension by comparing annual increase in tibia circumference directly from data with no interpolations (Supplementary Table 1). Ontogenetic body mass can also be determined. To do this, first the proportional relationship between tibia and femur length is calculated (Supplementary Table 1). A large, partially articulated *Maiasaura* specimen (ROM 44770) has a femur length of 102 cm and a fibula length of 98.5 cm (N. Campione personal communication 2013). Although ROM 44770 lacks a tibia, fibula length provides a

reasonable proxy. Tibia specimens of this size in our sample demonstrate the presence of an external fundamental system (EFS), so ROM 44770 is likely a skeletally mature individual. A body mass approximation of 3833 ± 958 kg (N. Campione personal communication 2013) for ROM 44770 was obtained from humerus and femur circumference measurements and using the phylogenetically corrected equation of Campione and Evans (2012). Our dataset consists only of tibiae, so we were unable to use the method of Campione and Evans (2012) to determine body mass for individuals in our sample. We instead used the developmental mass extrapolation equation (DME) of Erickson and Tumanova (2000) (but see Myhrvold 2013). This method interpolates body mass from femur length, provided an asymptotic adult mass is known (i.e., that of ROM 44770). By converting tibia circumference at each LAG to tibia length, and using the ratio of tibia to femur length from ROM 44770, annual femur length was determined for individual *Maiasaura* (Supplementary Table 1). From annual femur length, DME was used to calculate annual body mass (Supplementary Table 2).

As with the apposition rate calculations, the values represented by the periosteal surface for body size calculations (i.e., tibia circumference and body mass at death) are omitted from plots of immature individuals as the periosteal circumference does not represent a full year of growth. For the skeletally mature individual (T46) included in the body mass calculations, measurements based on the LAGs prior to the EFS (representing 9 years), as well as measurements based on the periosteal surface (representing year 13) are used, but the length and mass for the intervening years could not be calculated due to the difficulty of tracing complete line circumferences within the EFS. Additionally, crushed or missing outer cortex in some of the large tibiae made it impossible to fully trace multiple outer LAGs, so body sizes represented by these growth marks are omitted (Supplementary Table 1). The minimum diaphyseal circumference measurement of 2.5 cm from a perinate tibia (YPM-PU 22432) supplied data for time zero in regressions and body size calculations, and an estimated body mass of 2 kg (Horner et al. 2000) was used.

Tibia circumference and body mass growth curves of *Maiasaura* were constructed using the method of Lee and O'Connor (2013), which expanded the method of Cooper et al. (2008) to build a mean curve for multiple individuals. The circumference of each LAG was traced in Adobe Photoshop CS3, measured using the BoneJ (Doube et al. 2010) plugin for ImageJ (Rasband 1997–2014), and used to calculate tibia length and body mass as described above (Supplementary Tables 1–2). Because specimens needed to be over one year old and have complete, uncrushed diaphyseal cortex with fully traceable LAG circumferences, only nine tibiae could be used in constructing growth curves. Fitting model curves to the data for each specimen requires more than two LAGs, restricting the data set to five tibiae with uncrushed diaphyses and clearly traceable LAGs. Thus, although all nine well preserved post yearling tibiae are included on the growth curve graphs, only the five largest tibiae were used in constructing the growth curve models.

Rather than simply using the final tibia size and age at death, the method of longitudinally sampling (measuring the circumference at each LAG throughout the individual's life) provides repeated measurements of each individual (Lee and O'Connor 2013). These measurements are thus non independent, and so must be fitted to process error models (Cooper et al. 2008; Lee and O'Connor 2013; Lee et al. 2013). We used Equation 2 of Lee and O'Connor (2013), a reparameterized version of the Richards asymptotic growth model (Richards 1959):

$$C_{t+1} = A\left[1 + \exp(-K)\left[\left(\frac{C_t}{A}\right)^{1-m} - 1\right]\right]^{\frac{1}{1-m}}$$

As in Lee and O'Connor (2013), C_t is the size at time t, C_{t+1} is the size at time $t + 1$, "A is the asymptotic size, K is the mean relative growth rate, and m is the shape parameter" (Lee and O'Connor 2013: p. 868). By altering the value of m, this model converts into the monomolecular model ($m = 0$), von Bertalanffy model ($m = 2/3$), Gompertz model ($m = 1.001$), and logistic model ($m = 2$) (Lee and O'Connor 2013). These models were fit to the data for each tibia (the calculated diaphyseal circumference, tibia length, body length, or body mass at each LAG) using the nls (nonlinear least squares)

TABLE 2. *Maiasaura* growth model parameters and AIC_c values. An asterisk (*) indicates the optimum model for each dataset, having the lowest mean AIC_c value. Mean values are the average of values for the five tibiae with three or more LAGs (T33, T34, T36, T43, and T46). Abbreviations: m, shape parameter; A, asymptotic size in units listed in left-most column; K, relative growth rate per year; I, age in years at inflection point of growth curve; AIC_c, small-sample corrected form of Akaike's information criterion; ΔAICc, difference between AIC_c mean of each model and the model with the lowest AIC_c value.

Dataset	Model	m	A Mean	K Mean	I Mean	AICc Mean	ΔAICc
Diaphyseal Circumference (cm)	Monomolecular*	0	29.59	0.80	− 0.11	16.68	0.00
	Von Bertalanffy	2/3	28.64	1.25	0.41	24.50	7.82
	Gompertz	1.001	28.29	1.55	0.57	27.41	10.73
	Logistic	2	27.62	2.76	0.84	32.61	15.93
	Linear	na	na	4.34	na	36.33	19.65
Tibia Length (cm)	Monomolecular*	0	81.24	0.80	− 0.12	30.42	0.00
	Von Bertalanffy	2/3	78.68	1.23	0.40	37.96	7.54
	Gompertz	1.001	77.75	1.52	0.56	40.76	10.34
	Logistic	2	75.91	2.66	0.83	45.90	15.48
	Linear	na	na	12.17	na	50.13	19.71
Body Length (m)	Monomolecular*	0	5.89	0.85	− 0.11	− 4.21	0.00
	Von Bertalanffy	2/3	5.71	1.12	0.44	3.32	7.53
	Gompertz	1.001	5.64	1.51	0.56	6.12	10.33
	Logistic	2	5.51	2.66	0.83	11.27	15.48
	Linear	na	na	0.88	na	15.50	19.71
Body Mass (kg)	Monomolecular	0	6028.65	0.18	0.00	83.43	0.34
	Von Bertalanffy*	2/3	2337.36	0.69	1.44	83.08	0.00
	Gompertz	1.001	2185.78	1.09	1.78	90.12	7.04
	Logistic	2	2254.69	1.05	6.71	94.41	11.33
	Linear	na	na	10.83	na	98.63	15.55

function in R 2.11.1 for Mac OS X (R Development Core Team 2010) and R scripts we adapted from those of Cooper et al. (2008; provided by A. Lee, personal communication 2013). Our modified version of the Cooper et al. (2008) R scripts can be found in Supplementary Document 1.

These R scripts were run for each tibia and repeated for each type of data: tibial circumference, tibial length, body length, and body mass (Supplementary Document 1). For each model type and data type, the results for the five individual tibiae were averaged to yield mean values for *A*, *K*, AIC_c, and residual standard error; e.g., the five individual results for the tibial circumference monomolecular model were averaged (Table 2). The goodness of fit of the models was determined by the mean AIC_c (Akaike's Information Criterion, small sample corrected form) and mean residual standard error; the model type with the lowest mean AIC_c and mean residual standard error was selected as the best fit to the data (Lee and O'Connor 2013); different data types were best fit by different model types (Table 2). After the best model type for each data set was selected, its previously calculated mean values

for *A* and *K* were then used in the model equation to produce a mean growth curve for each graph (Fig. 2, Supplementary Fig. 2). This mean curve was parametrically bootstrapped (2000 replicates) using the mean residual standard error to produce 95% confidence intervals for the mean curve (Lee and O'Connor 2013) (Table 3).

Myhrvold (2013) suggested that many published dinosaur ontogenetic body mass curves are fraught with errors in calculations or rely on largely untested mass interpolation methods (including DME, used here). Even if this were not the case, most dinosaur body mass curves are derived from linear measurements, providing ample opportunities for volumetric scaling errors (see Lee et al. 2013). Also, due to the complete lack of associated skeletal elements in the *Maiasaura* bonebed, we must assume that tibia and femur lengths increased isometrically in order to apply the DME to femur lengths estimated from tibia lengths. A study on *Maiasaura* by Dilkes (2001) does suggest isometry of the hindlimb, but Kilbourne and Makovicky (2010) suggest positive allometric growth. Because of the many potential sources of error, body mass curves in Figure 2B should
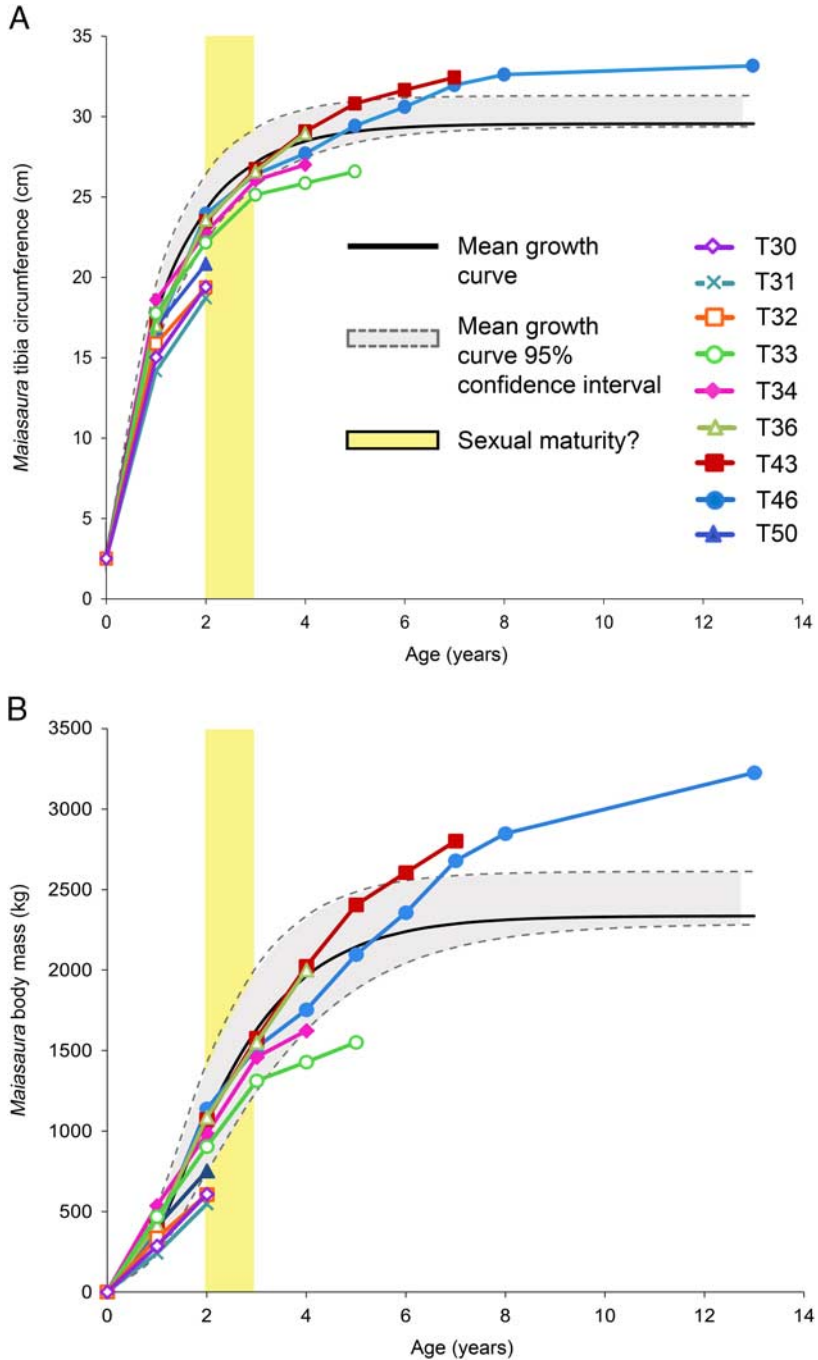
FIGURE 2. Growth curves for *Maiasaura peeblesorum*. Age in years (determined by the number of LAGs) is plotted against size: A, tibial minimum diaphyseal circumference, B, body mass. The monomolecular model was used to plot mean tibial diaphyseal circumference, whereas the von Bertalanffy model was used to plot mean body mass. Mean curves were fitted based on the five largest tibiae included in the graph; the four smaller tibiae with only two LAGs did not have enough data points to fit the models. The 95% confidence intervals are based on mean residual standard error around the mean curve, not the individual curves. Yellow bar indicates hypothesized age at which individuals would become sexually mature.

TABLE 3. The 95% confidence intervals around *Maiasaura* mean growth curve model parameters. The 95% confidence intervals were calculated using parametric bootstrapping on the mean residual standard error. Mean values are the average of values for the five tibiae with three or more LAGs (T33, T34, T36, T43, and T46). Abbreviations: m, shape parameter; A, asymptotic size in units listed in the Dataset column; K, relative growth rate per year; I, age in years at inflection point of growth curve. "Time to 95% Max Size" indicates the age in years at which 95% of asymptotic size is reached.

Dataset	Model	m	Line	A	K	I	Time to 95% Max Size (years)
Circumference (cm)	Monomolecular	0	Mean	29.59	0.80	− 0.11	3.64
			lower 95%	29.42	0.65	− 0.13	3.31
			upper 95%	31.35	0.88	− 0.10	4.45
Tibia Length (cm)	Monomolecular	0	Mean	81.24	0.80	− 0.12	3.65
			lower 95%	80.64	0.65	*− 0.14*	3.34
			upper 95%	86.27	0.87	*− 0.11*	4.48
Body Length (m)	Monomolecular	0	Mean	5.89	0.85	− 0.11	3.42
			lower 95%	5.86	0.69	− 0.13	3.12
			upper 95%	6.25	0.93	− 0.10	4.22
Body Mass (kg)	Von Bertalanffy	2/3	Mean	2337.36	0.69	1.44	5.76
			lower 95%	2288.72	0.53	1.24	4.97
			upper 95%	2613.83	0.80	1.88	7.51

therefore be considered with caution. Despite these caveats, the growth history of an animal is best illustrated in three dimensions and we include body mass curves here to illustrate a generalized volumetric growth trajectory for *Maiasaura*, and to allow comparisons with ontogenetic body mass curves published for other dinosaur species.

To complement growth curves derived from tibia and femur lengths here and elsewhere, and to circumvent the allometric versus isometric growth problem, we present a novel method to directly compare growth rate data across various taxa. *Maiasaura* tibia annual cross sectional cortical area growth was plotted against cumulative cross sectional cortical area and normalized by the largest skeletally mature values in the sample. This normalization results in quantifiable measurements from *Maiasaura* individuals plotted on a dimensionless scale from 0% to 100% maximum size, with no need for potentially erroneous body size calculations. The same method was applied to a sample of twelve *Alligator mississippiensis* femora of known ages: ten captive male *Alligator mississippiensis* femora, representing nine skeletally mature 26 and 27 year old individuals with EFS (Woodward et al. 2011) and one immature individual at least eight years of age; and two immature 5 year olds, one of which does preserve the first LAG, yielding size at age 1 year (Woodward et al. 2014). A perinate *Alligator* femur was also measured to provide femur size at hatching. Because cortical measurements are normalized, the *Alligator* and *Maiasaura* data could be plotted on the same graph and comparisons of annual cortical thicknesses made (Fig. 3). The innermost LAGs of the skeletally mature alligators had been destroyed by medullary expansion, so that the first data point for each line is not that of the first LAG but instead marks an average of approximately the seventh year of growth. Because the growth marks within an EFS are so closely spaced, accurately measuring the annual cortical growth is extremely difficult, so the cortical area within the entire EFS was divided by the number of growth marks, yielding equal annual growth for each year represented by the EFS. Although no alligator tibiae were available for comparison, results from Woodward et al. (2014) demonstrate that *Alligator mississippiensis* femur cortical thickness increases are comparable to tibia cortical thickness increases, and that the femur and tibia are amongst the fastest growing alligator limb elements. In turn, Farlow et al. (2005) show that *Alligator* femoral dimensions including midshaft circumference can be used to predict total length. The dataset from Farlow et al. (2005) also reveal a tight correlation between femoral midshaft cortical area and body mass (Supplementary Figure 3). Although *Maiasaura* and *Alligator* have very different body plans and ontogenetic limb allometries,
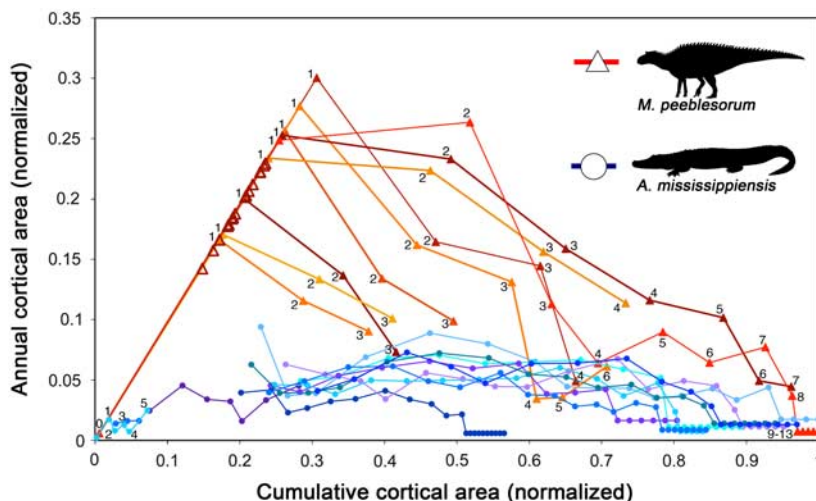
FIGURE 3. Annual growth of cross sectional cortical area in *Maiasaura* and *Alligator*. The y-axis represents the increase in cross sectional cortical area over a single year *t*, and the x-axis represents the total cross sectional cortical area at year *t*. Both axes are normalized so that the cross sectional cortical area at death of the largest sampled individual for each taxon equals 1. The LAG age of each *Maiasaura* data point is indicated next to its triangle. Individuals that died during their first growth hiatus are indicated by open triangles. The only *Alligator* specimen to preserve the first LAG has the LAG number of each data point indicated next to its circle. *Maiasaura* have the greatest cortical area growth in their first year, with annual growth steadily decreasing; 95% of growth is completed by 7 to 8 years of age. *Alligator* have a proportionally slower, steadier growth of cortical area. All but three *Alligator* specimens were 26 to 27 years of age at time of death; the largest individual completed 95% of its growth by 23 to 24 years of age. The spread of lines for each taxon demonstrates individual variation in body size and growth rate. If an individual had an EFS, this is indicated on the graph by a horizontal series of equally spaced points. The locations of the *Alligator* EFS segments along the x-axis demonstrate individual variation in asymptotic body size relative to the largest specimen.

tibiae and femora are still amongst the fastest growing elements in both taxa and reliably reflect body size increases. Regardless, our method must still be used with caution as it is susceptible to differing allometries across taxa, but it may be used to complement body mass curves by offering another way to compare growth in different taxa.

Results

Predicting *Maiasaura* tibia medullary cavity circumference and area from tibia length (or vice versa) is not reliable ($R^2 = 0.79$), indicating some variability in medullary cavity values associated with similar tibia lengths (Supplementary Tables 5–6). There is, however, a strong linear relationship between tibia length and diaphyseal circumference ($R^2 = 0.95$; $y = 0.3685x - 0.2654$) (Supplementary Table 4), and a strong exponential relationship between tibia length and total cortical area ($R^2 = 0.96$; $y = 3.5948e^{0.0335x}$) (Supplementary Table 7), as well as tibia length and diaphyseal bone wall

thickness ($R^2 = 0.97$; $y = 3.8309e^{0.0309x}$) (Supplementary Table 8).

Throughout ontogeny, the diaphyseal cortex is made of well vascularized woven fibered tissue (Fig. 4A). Only in the outermost cortex of the largest tibiae in the sample does vascularity decrease and tissue fiber become organized in parallel (Fig. 4E). As observed by Horner et al. (2000), the vascular pattern found in young tibiae (up to LAG 2) is largely a mix of laminar and reticular, becoming increasingly sub plexiform to plexiform after the second LAG. We also confirm the observations of Horner et al. (2000) that vascular organization changes frequently about the cortex. Secondary osteon density within the cortex is minimal throughout the sample. Rather, multiple generations of secondary osteons are found in a narrow, radial strip or "anterolateral plug" (sensu Hübner 2012) from innermost cortex to the periosteal surface near the anterior tibial border in larger tibiae. These secondary osteons are located in larger tibiae where a column of radial vascularity exists in smaller
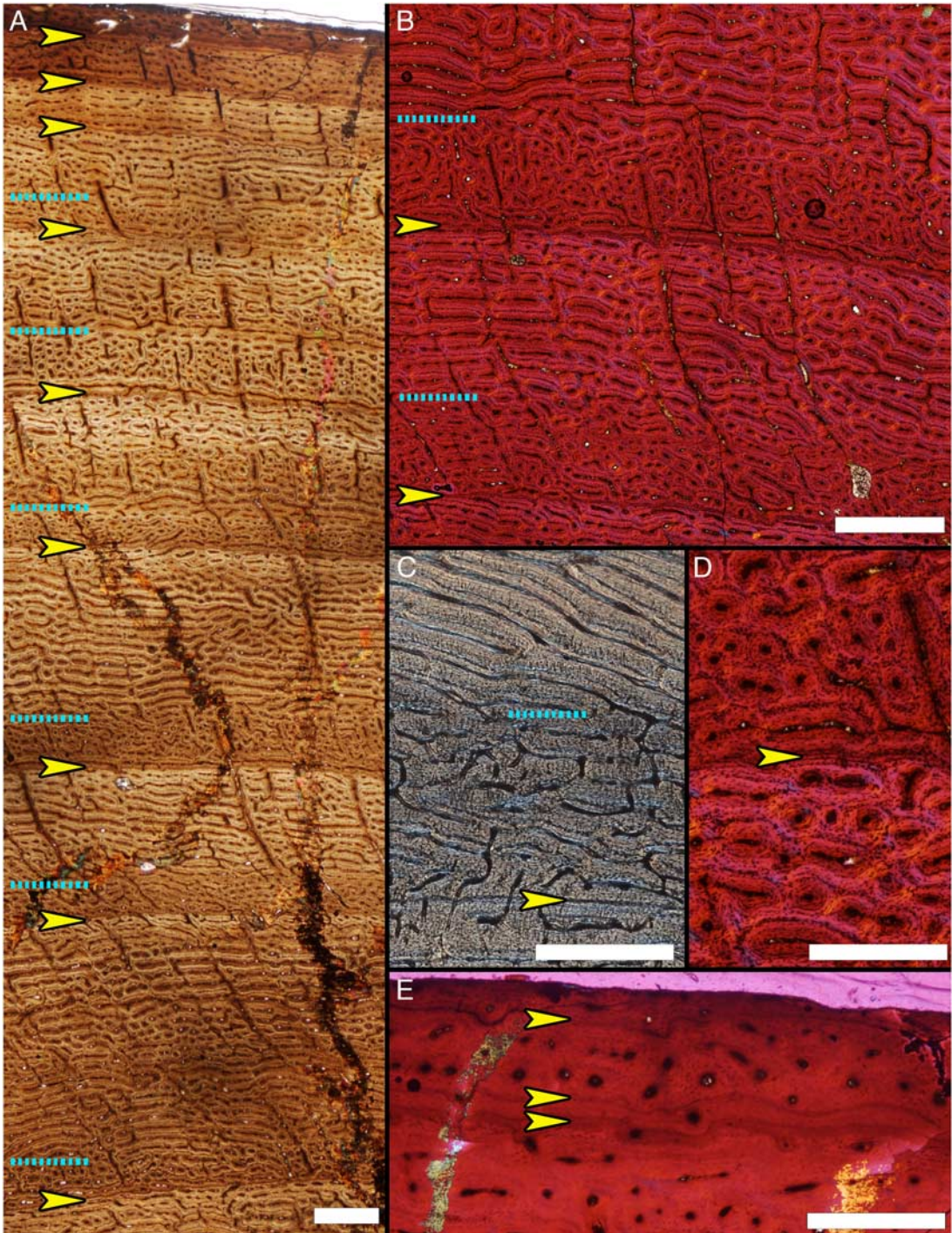
FIGURE 4.   Vascular cyclicity, LAGs, and an external fundamental system (EFS) from the diaphyseal midshaft of *Maiasaura* tibia T46. A, Lateral radial transect from inner cortex (bottom) to the periosteal surface (top). The lowermost arrow indicates LAG 2. Dotted lines mark the shift from predominately reticular vascularity immediately following a LAG (arrow) to laminar or plexiform vascularity prior to the subsequent LAG. Polarized light. Scale bar, 1mm. B, The mid cortex of (A) at higher magnification detailing the cyclical change in vascularity (dotted lines) within the zones bounded by LAGs 3 and 4 (arrows). 540 nm wave plate. Scale bar, 1 mm. C, Cortical microstructure from a red deer (*Cervus elaphus*) (image courtesy of M. Köhler) showing a LAG (arrow) as well as a zonal transition (dotted line) in vascular organization, similar to what is observed in *Maiasaura*. Scale bar, 500 μm. D, LAGs (arrow) in *Maiasaura* tibiae are very thin and easily overlooked. 540 nm wave plate. Scale bar, 500 μm. E, The EFS (arrows) at the periosteal surface showing three closely spaced LAGs within an organized matrix and longitudinal vascular canals. 540 nm wave plate. Scale bar, 500 μm.

tibiae, and both the radial primary tissue as well as the remodeled secondary tissue "plug" is most likely related to a tendonous insertion near the anterior tibial border.

The rapidly deposited, woven fibered cortical matrix of *Maiasaura* tibiae examined in this study often contains lines of arrested growth (LAGs; Fig. 4). Much like rings within a tree trunk, LAGs indicate annual pauses in appositional growth (e.g., Peabody 1961; Köhler et al. 2012), allowing the ageing of *Maiasaura* individuals. The LAGs in *Maiasaura* tibiae are identified as thin black lines within the primary cortical tissue. Unless obfuscated by secondary remodeling or missing/damaged cortex, LAGs are fully traceable about the circumference of the section, are parallel to each other, and in general become more closely spaced near the outer cortex of larger individuals.

Tibia lengths for individuals approaching one year of age range between 29.4 cm and 48.8 cm (Fig. 1), with diaphyseal circumferences 14.3–18.3 cm. Size variation continues throughout ontogeny, with tibia lengths between 56–69.5 cm and corresponding diaphyseal circumferences of 21.4–26.5 cm by the third year of life. Tibia length (75–88 cm) and circumference (28–33 cm) begin to plateau between the sixth and eighth year of life. No tibiae 49–55.5 cm in length or 70–75 cm in length are present in the sample. In the largest tibiae, medullary expansion and secondary osteons only partially destroy the first LAG.

At low magnification (10× total) even the cortices of some of the smallest tibiae examined (33.8–48.8 cm in length) appear to have LAGs. But close examination at higher magnification (40× to 100× total magnification) reveals concentric bands of localized changes in the diameter and orientation of vascular canals (Fig. 5). True LAGs first appear in thin sections from tibiae 56 cm in length and larger (Fig. 4), but no tibiae in the sample possess only a single LAG and tibiae with only three LAGs are also absent. Specimens 56–69.5 cm in length all possess two LAGs and those 75–99.7 cm in length have between four and ten LAGs (Fig. 1, Supplementary Table 1). The tibiae 75 cm in length and larger also have progressively more closely spaced LAGs nearing the periosteal
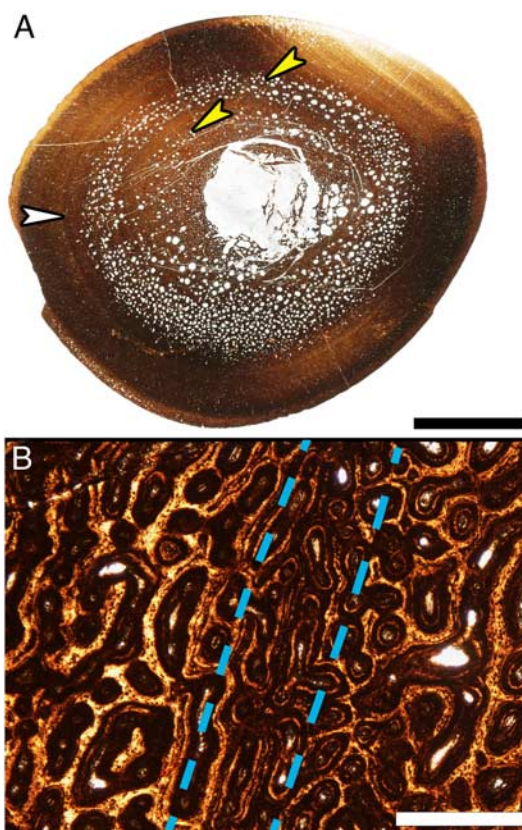

FIGURE 5. Resorption cavity rings and localized vascular changes within the cortex of a *Maiasaura* tibia (T16) approaching one year of age. A, Mid diaphyseal transverse section with two resorption cavity rings (yellow arrows) within the cortex. The white arrow indicates a ring within the cortex that could be mistaken for a line of arrested growth (LAG). Scale bar, 1 cm. B, Enlargement of the region indicated by the white arrow in (A), centered on the ring visible within the cortex (between dashed lines). At this magnification it becomes apparent that the ring is formed by a localized change in vascular canal size and that no LAG is present. Scale bar, 500 µm.

surface, with five tibiae being skeletally mature as revealed by the presence of an external fundamental system (EFS). By utilizing the regression equation resulting from plotting tibia length against diaphyseal circumference ($y = 0.3685x - 0.2654$), the first (innermost) LAG circumference measurements from tibiae 56 cm in length and greater reveal lengths between 39 cm and 51 cm at the close of the first year of growth (Supplementary Table 2).

Based on the complete absence of LAGs, 31 tibiae within the sample set represent individuals less than one year of age. Thus, *Maiasaura*
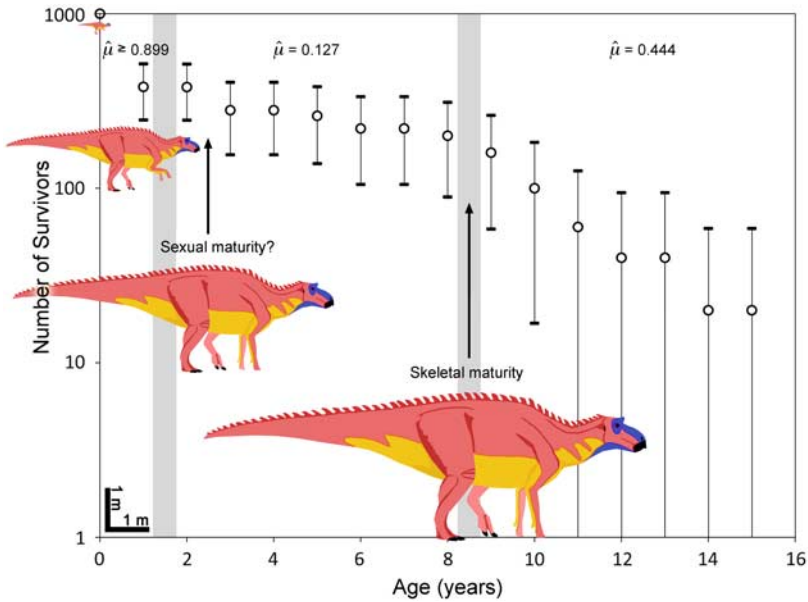
FIGURE 6. Survivorship curve for *Maiasaura*. Sample size of 50 tibiae was standardized to an initial cohort of 1000 individuals (assumes 0% neonate mortality). Survivorship is based on the number of individuals surviving to reach age *x* (the end of the growth hiatus marked by LAG *x*). Age at death for individuals over 1 year old was determined by the number of LAGs plus growth marks within the EFS, when present. Error bars represent 95% confidence interval. Mean annual mortality rates ($\hat{\mu}$) given for age ranges 0–1 years, 2–8 years, and 9–15 years. Vertical gray bars visually separate the three mortality rate age ranges.

young of the year mortality rate is high (≥89.9%). After the first year, mortality rate sharply decreases (Fig. 6). There is a brief increase in mortality rate between years 2 and 3. By dividing the non juvenile (i.e., 2 or more years of age) *Maiasaura* into two age groups, the mortality rates of those age groups can be compared. The non juvenile age groupings with the greatest difference in mortality rates (and smallest 95% confidence interval) are 2–8 years old (mean annual mortality rate 12.7%) compared with 9–15 years old (mean annual mortality rate 44.4%), indicating that a second period of elevated mortality begins between 8 and 9 years of age.

A large portion of early rapid growth was achieved during the first year, with bone apposition rate averaging 65.1 µm/day, decreasing to 21.4 µm/day in the second year, and falling again in the third year to 13.7 µm/ day (Table 1). By the ninth year, average apposition rate declines to 2.6 µm/day. Despite annual apposition rate reductions, in the zones of cortex separated by LAGs, fiber orientation is woven and the tissue is well

vascularized throughout most of ontogeny (Fig. 4A). Reticular, sub laminar, and laminar vascularity predominates in smaller tibiae (<70 cm in length), and a greater proportion of laminar and plexiform vascularity occurs in larger specimens (>70 cm in length). However, even when observing similar locations around the cortex, vascular canal orientation differs among same size tibiae as well as ontogenetically.

Within the woven fibered zones of the cortex, two peculiar patterns of resorption and vascularity present themselves. The first are concentric resorption cavity rings in the mid cortex of tibiae between 40 cm and 50 cm in length (i.e., young of the year) (Fig. 5A). The second unusual vascular arrangement begins in larger tibiae: immediately following the second LAG, vascular canals are initially reticular corresponding to high apposition rates (average 31.6–33.2 µm/day in ratites (Castanet et al. 2000)). Then the vascular pattern transitions to laminar or plexiform with somewhat lower apposition rates (average 24.7–27.1 µm/day in ratites (Castanet et al. 1996;

Castanet et al. 2000)) for the majority of the zone (Fig. 4A, B). The progression from reticular to dominantly laminar or plexiform then repeats within each successive zone, but becomes less prevalent in the more closely spaced zones immediately prior to the EFS. This repeating vascular pattern is consistently seen in posterior orientation of the cortex, and may be less pronounced or even absent at other locations about the transverse section.

For modeling tibia circumference and body mass curves, the monomolecular model was the best fit (lowest mean AIC_c) for the former, and the von Bertalanffy model was the best fit for the latter (Table 2). Figure 2A and 2B plot the circumference and mass curves (respectively) for each of the nine individuals for which enough LAGs were preserved, but only the five largest tibiae of the nine were used to model the mean growth curves. Individual tibiae display a range of individual body size variation; the mean curve represents the mean of the model curves fit to each of the individual tibiae. The difference between the fit of each model curve and the actual individual data points is represented by the residual standard error. The mean of the residual standard error was used to construct the 95% confidence intervals around the mean curve (see Methods). Thus, the 95% confidence intervals represent a range of variation around the mean line that would contain 95% of data points if the mean line were constructed from an actual tibia instead of an idealized perfect curve model. Individual body sizes may be smaller or larger than this mean curve and its confidence intervals; the growth trajectory of a smaller bodied individual would resemble a slightly scaled down version of the mean curve and confidence intervals, and a larger bodied individual would resemble a slightly scaled up version.

According to the mean growth curve model, mean body mass and tibia diaphyseal circumference at the close of the first year of growth is 384.3 kg and 17.4 cm respectively, and increases to 1632 kg and 27.1 cm by the end of the third year of growth (LAG 3). Growth begins to plateau after LAG 8 as the mean asymptotic body mass of 2337.4 kg and tibia circumference of 29.6 cm is approached.

Discussion

Cyclical Growth Marks.—The diaphyseal cortices of tibiae 33.8–48.8 cm in length appear to possess LAGs. However, examinations at higher magnifications reveals that these structures are instead concentric rings of localized changes in vascular canal orientation and diameter (Fig. 5), and were previously described in *Maiasaura* elements categorized as juvenile by Horner et al. (2000). We agree with the original conclusion that such localized vascular fluctuations are the result of changes in bone apposition rate and not of arrested growth, and that more research on extant bone tissue growth is needed to understand their cause before they could be interpreted as annual growth marks in very fast growing bone. On the other hand, the cortex of every tibia 56 cm in length and larger contains true LAGs. Even at tibia lengths of 75 cm and greater, continued medullary expansion and frequent secondary osteons only partly destroy the innermost LAG. Calculated tibia lengths corresponding to the circumference of the first (innermost) LAG in tibiae 56 cm or larger are between 39 cm and 51 cm (Supplementary Table 2). A LAG becomes visible after growth resumes, so specimens from the sample without LAGs, but between 39 cm and 51 cm in length, therefore represent individuals that perished while experiencing their first annual growth hiatus and illustrate the size variability already present at this young age.

The thickness of cortical zones between each LAG represents yearly bone apposition that, in the *Maiasaura* tibia cortices, progressively decreases with increasing age. Reduction in yearly cortical apposition (and therefore growth rate) is especially apparent in tibiae 75 cm in length or greater (>7 LAGs), and such pronounced reduction is associated with nearing skeletal maturity.

By retro calculating missing LAGs to construct a growth history, and also by using experimentally obtained growth rate estimates for various limb bone types in extant taxa, Horner et al. (2000) estimated that *Maiasaura* attained skeletal maturity in six to eight years. Of the eleven tibiae in our sample with at least 7 LAGs, five (45.4%) possess an external

fundamental system (EFS) in the outermost cortex (Fig. 4E). In extant vertebrates, the EFS is associated with attainment of skeletal maturity as it signals the effective cessation of long bone increase in length (Cormack 1987; Castanet et al. 1988). The mean age at which skeletal maturity occurred in the five individuals with EFS is 8.25 years, which supports the original estimate of six to eight years by Horner et al. (2000). The remaining six tibiae with at least 7 LAGs (54.5%) are a mean age of 8.7 years but lack an EFS, revealing individual variation not only for the age at which skeletal maturity occurs, but also in corresponding tibia lengths at skeletal maturity. For instance, two tibiae, both with 8 LAGs prior to their EFS, have respective tibia lengths of 75 cm and 87.5 cm. But a third tibia 90 cm in length has 10 LAGs and no EFS, indicating that at ten years of age this individual was still growing. Further variability in age and tibia length at skeletal maturity will likely manifest as additional large specimens are incorporated into the sample.

Survivorship, Maturity, and Longevity.— Dinosaur population survivorship has been previously modeled for *Albertosaurus, Gorgosaurus, Daspletosaurus, Tyrannosaurus,* and *Psittacosaurus* (Erickson et al. 2006; Erickson et al. 2009; Erickson et al. 2010). Unfortunately, due to the difficulty presented by fossil scarcity and in obtaining multiple specimens for histological sampling, such modeling has been criticized for its lack of biologically statistically significant sample sizes (Steinsaltz and Orzack 2011). The minimum number of specimens required to construct meaningful survivorship curves was suggested as 50 in a critique of *Albertosaurus* survivorship curves by Steinsaltz and Orzack (2011). Although far from the hundreds or thousands of individuals comprising modern vertebrate and invertebrate survivorship studies, the 50 *Maiasaura* tibiae of known (rather than estimated) age utilized in our sample is the largest yet for any dinosaur taxon; meets the minimum sample number advocated by Steinsaltz and Orzack (2011) for survivorship studies; and is the first to incorporate an entire ontogenetic series from hatching to skeletal maturity with no age estimation or retro calculation. It is important

to note, however, that our *Maiasaura* sample set is highly atypical for fossil taxa (especially dinosaurs). Due to the likelihood of fossil tetrapod preservation, paleontologists are commonly restricted to small numbers of fossils for any kind of research. Thus, a prerequisite of at least 50 fossil specimens for population analyses is unreasonable for most extinct tetrapod taxa. When viewed in this way, the *Maiasaura* sample is a fortunate exception, providing valuable insights into the population biology of an extinct animal.

Varricchio and Horner (1993) reported a skeletal element length frequency distribution for the *Maiasaura* bonebed that included humeri (n = 20), tibiae (n = 16), and femora (n = 18). Based on size distribution, they concluded there was high juvenile mortality and predicted that the majority of the sample was made of young of the year. Our age frequency distribution of *Maiasaura* also suggests age specific mortality biased towards the very young as well as senescent attrition, rather than representing an accurate profile of the living population structure (Fig. 1) (Voorhies 1969; Varricchio and Horner 1993; Erickson et al. 2010). The combination of *Maiasaura* high initial mortality followed by a period of low mortality, and eventually ending in senescent attrition, closely resembles the sigmoidal B1 type survivorship curve (Pearl and Miner 1935), which is frequently associated with a survivorship study by Deevey (1947) on Dall sheep (*Ovis dalli*). Although the B1 survivorship pattern has been suggested for other dinosaur groups (*Albertosaurus, Gorgosaurus, Daspletosaurus, Tyrannosaurus,* and *Psittacosaurus*; Erickson 2006; 2009), ours is the first study to demonstrate this B1 pattern utilizing individuals ranging from hatching and less than one year of age through skeletal maturity, with no retrocalculations or estimations of age.

A modern analogue to *Maiasaura* survivorship presents itself in a red deer (*Cervus elaphus*) population from the Isle of Rum, Scotland. Of the many ongoing mammal and bird population studies, we chose to use the Isle of Rum red deer as analogues for interpreting *Maiasaura* survivorship patterns due to the data available to support the red deer ecological interpretations: The Isle of Rum Red

Deer Project (http://rumdeer.biology.ed.ac.uk/) is one of the longest running (since 1953) scientific studies of a vertebrate population in the world. Over sixty years of research on this population results in detailed studies on pedigree, behavior, life history trade offs, and survivorship. In addition to the accumulated Isle of Rum data, red deer are acceptable analogues because of the similarities not only between *Maiasaura* and red deer survivorship curve type (B1), but also in bone tissue organization: woven bone tissue separated by growth marks in both taxa indicates high sustained growth rates occurring over a period of years (Fig. 4C); furthermore, both taxa are relatively large bodied quadrupedal herbivores.

Thirty one of the fifty *Maiasaura* tibiae examined here lack LAGs, meaning that young of the year make up over half of our sample (Fig. 1). This signal is also reflected in the frequency distribution of *Maiasaura* femora from the bonebed, as 13 of the 18 femora (72%) included in a limb frequency analysis by Varricchio and Horner (1993) were less than 50 cm in length, and femora of this length represent young of the year according to the analysis by Horner et al. (2000). The corresponding mean mortality rate for the first year of growth based on the tibiae in our sample is at least 89.9%. After the first year of life the mean mortality rate falls to 12.7% (Fig. 6). For the red deer population, juvenile mortality is highest during the first two winters after weaning, when the animals may succumb to the high energy costs of rapid growth during a period of reduced resources (Clutton-Brock et al. 1985; Catchpole et al. 2004). In extant alligators as well as ruminants such as the red deer, the annual growth hiatus occurs during unfavorable months when resources are less plentiful (Joanen and McNease 1987; Köhler et al. 2012). Perhaps the annual *Maiasaura* growth hiatus also corresponded to a seasonally stressful period, during which time the young of the year were particularly susceptible to predation, starvation, exposure to weather, or other external factors, increasing the mortality rate for this age group.

In contrast to the high number of early juveniles present in the *Maiasaura* sample, those between one and two years of age

(yearlings) are absent (Fig. 1). In other words, no tibiae possess only a single LAG. Horner et al. (2000) found the same to be true of the six femora included in their *Maiasaura* ontogenetic histologic analysis: the "late juvenile" category femur (50 cm in length) lacked LAGs, and the next largest (68 cm) already had two LAGs. That the absence of individuals between one and two years of age is recorded in both femora and tibiae adds support to our hypothesis that yearlings were rarely incorporated into the bonebed. Thus, it seems that if young *Maiasaura* could endure their first unfavorable season, the chances of surviving another year were high. A slight increase in mortality occurred between 2 and 3 years of age (2 LAGs), which may signal attainment of sexual maturity (Erickson et al. 2006, 2010) and the accompanying increased physiological demands related to breeding and/or competition for mates (Fig. 6). The complete absence of three and four year olds (3–4 LAGs; Fig. 1) from the sample suggests that individuals able to withstand the onset of this additional stress would likely live into their fifth year before mortality began to rise again, which is reflected in the mean mortality rate of only 12.7% for *Maiasaura* between 2 and 8 years of age (Fig. 6). Such a mortality plateau is also exhibited by the Isle of Rum red deer. For red deer, this period begins around the third year of life coinciding with sexual maturity onset and marks a time of peak performance, when survival and reproductive success are highest (Catchpole et al. 2004; Nussey et al. 2009).

A second period of elevated mortality in *Maiasaura* begins between eight and nine years of age (44.4% mean annual mortality rate; Fig. 6). The mortality rate of Isle of Rum red deer also rises between eight and nine years of age, as they enter a period of senescence, defined by Jones et al. (2008) as "a decline in fitness with age caused by physiological degradation" (p. 665). For *Maiasaura*, eight years coincides with mean age at skeletal maturity, supporting a senescence correlated increase in mortality.

The B1 survivorship pattern observed in *Maiasaura* – presumed high juvenile mortality, followed by a mortality plateau, and lastly elevated adult mortality – was previously reported for the basal ceratopsid *Psittacosaurus*

(Erickson et al. 2009) and for the tyrannosaurid *Albertosaurus* (Erickson et al. 2006, 2010). The same B1 pattern recorded in the Isle of Rum red deer population was used to support the antagonistic pleiotropy theory of ageing, which states that achieving sexual maturity early in life reduces reproductive performance and survival probabilities later in life (Nussey et al. 2008). Red deer studies also suggest that the magnitude of senescence is directly related to early development; essentially, animals that achieve peak performance early, senesce quickly (Jones et al. 2008). These hypotheses explain the survivorship curves exhibited by *Maiasaura*, *Psittacosaurus*, and *Albertosaurus*: the dinosaurs grew rapidly to attain the minimum body size necessary to escape strong environmental and predatory pressures (Cooper et al. 2008), and achieved peak performance relatively early in ontogeny (sensu Albon et al. 1987). The consequence for high energy demands early in ontogeny is high juvenile mortality followed by rapid senescence after the peak performance window (Jones et al. 2008). If proportionally few dinosaurs in a population survived beyond the onset of sexual maturity (only 28% in our *Maiasaura* sample), and mortality related to senescence rose immediately following the peak performance plateau, this may explain why exceptionally large, skeletally mature dinosaurs with thick EFS are rare in the fossil record (e.g., Erickson 2005; Erickson et al. 2006; Erickson et al. 2009; Horner et al. 2011).

Apposition Rates and Ontogenetic Growth.— The bone apposition rate in *Maiasaura* was highest during the first year of life, with a mean of 65.1 μm/day, falling to 13.7 μm/day by the third year of life and presumed onset of sexual maturity (Table 1). Continued body size increase likely remained advantageous after reaching sexual maturity, but proceeded at lower rates approaching an asymptote; average apposition rate declined annually to 2.6 μm/day by year nine. Although apposition rate steadily declined over ontogeny, woven bone continues to be deposited until skeletal maturity was achieved (Fig. 4). Vascular orientation did change throughout ontogeny, with reticular, sub laminar, and laminar vascularity common in smaller tibiae (<70 cm

in length), and increased amounts of laminar and plexiform vascularity in larger specimens (>70 cm in length). Differences in vascular orientation about the cortex within a woven fibered matrix may indicate either changes in mechanical loading (de Margerie et al. 2002) or apposition rates (de Margerie et al. 2004), although the two are not mutually exclusive. Regardless, the variability in vascular arrangement among the smallest specimens, combined with a cyclically repeating vascular pattern observed within zones of older individuals (see below), shows that in *Maiasaura* ontogenetic vascularity changes were influenced most strongly by growth rate fluctuations.

Among extant archosaurs, woven fibered tissue is only extensively present in Aves, where apposition rates range between 5 μm/ day to 171 μm/day, but with considerable overlap in rates for different vascular arrangements (Castanet et al. 1996; Castanet et al. 2000; de Margerie 2002; de Margerie et al. 2002; Starck and Chinsamy 2002; de Margerie et al. 2004). For instance, avian histology studies report that, depending on species and skeletal element, the range of average apposition rates are between 10 μm/day and 39.5 μm/day for reticular, laminar, sub laminar, and sub plexiform vascularity (Castanet et al. 1996; Castanet et al. 2000); 4.8–50 μm/day for longitudinal vascularity (Castanet et al. 2000; Starck and Chinsamy 2002); and 5–15 μm/day for plexiform (Castanet et al. 1996). Density of vessels decreases below a rate of 5 μm/day, and below 1 μm/day vascularity disappears and parallel fibered tissue dominates (Castanet et al. 1996). After the fifth year of life *Maiasaura* average apposition rates generally fall below 3 μm/day within the realm of decreased vascularity and parallel fibered organization. These rates are counterintuitive since qualitative observation shows cortical tissue remains consistently well vascularized and woven for several additional zones prior to the EFS (Fig. 4). Somewhat higher average annual apposition rates result by incorporating the growth hiatus into apposition estimates. This method has not previously been applied to dinosaurs, but can be demonstrated using extant taxa (Joanen and McNease 1987; Castanet et al. 1988). For instance, the

growing season for alligators in Louisiana is approximately seven months (Joanen and McNease 1987) and so their average annual apposition rates should be based on a growing season of 214 days rather than 365 days. The duration of the growth hiatus in *Maiasaura* is unknown, but we conservatively estimate a minimum of three months as determined for extant ruminants (Köhler et al. 2012). A comparison beyond the archosaurian extant phylogenetic bracket is justified here as ruminant bone microstructure consists of rapidly growing tissue separated by LAGs (Fig. 4C), therefore resembling *Maiasaura* tissue organization more closely than that of either crocodylians (no extensive woven tissue) or birds (most take less than a year to reach skeletal maturity (Castanet 2006)). Using this approach, the average daily apposition rate of *Maiasaura* prior to the first hiatus was 86.4 μm/day; 28.4 μm/day for yearlings; 18.2 μm/day during the third year; and falling to 3.5 μm/day by the ninth year (Table 1). These adjusted apposition rates consider the yearly growth hiatus and remain within the recorded range for woven, well vascularized avian tissues for most of ontogeny, while also tracking the decrease in vascularity occurring in the zones immediately preceding the EFS in the largest specimens.

The vertebrate growth hiatus is still not fully understood, requiring further research on extant vertebrates. A novel approach is to explore whether growth hiatus duration lengthens with increasing age, since duration changes by latitude and with photoperiod manipulation (Joanen and McNease 1987; Lance 1989; Wilkinson and Rhodes 1997; Castanet et al. 2004). If yearly apposition rate was constant while the growth hiatus increased during *Maiasaura* ontogeny, the high first year apposition rates (57.0–100.9 μm/day) could be sustained throughout growth (Table 1). These rates are well within the range observed in extant Aves, while offering a novel alternative hypothesis to explain how tissue organization remained woven throughout ontogeny even as zone thickness progressively decreased. Actual *Maiasaura* growth may have combined a decrease in apposition rate with an increase in duration of the growth hiatus, thus falling between the extremes bracketed in Table 1.

Comparative Analysis of Apposition Rates.— The appositional growth rate data acquired from *Maiasaura* are useful not only for a deeper understanding of its growth history, but also for growth rate comparisons across taxa. As an example, normalized *Maiasaura* tibia cortical growth was plotted alongside normalized *Alligator mississippiensis* femur cortical growth (Fig. 3), with the simple purpose of testing the hypothesis that the growth histories of these two archosaur taxon will exhibit marked differences when directly compared in a normalized fashion. Alligators are a very well studied group histologically, and are often utilized to understand zonal bone growth in dinosaurs (e.g., Erickson 1996; Farlow and Britton 2000; Farlow et al. 2005; Schweitzer et al. 2007; Tumarkin-Deratzian 2007; Tumarkin-Deratzian et al. 2007; Klein et al. 2009; Farmer and Sanders 2010; Woodward et al. 2011, 2014). The seemingly obvious comparison of dinosaur histology to that of their extant bird descendants does not apply here, because (with few exceptions), extant birds achieve adult size in less than a year and therefore do not deposit zonal bone. The 12 alligators used in this comparison were captive raised and therefore possessed growth rates much higher than their wild counterparts, and the nine oldest specimens had in fact attained skeletal maturity before their 26th year of life (Woodward et al. 2011). Unfortunately, *Alligator* tibia data were not available to compare directly to *Maiasaura* tibia data. However, Woodward et al. (2014) demonstrate that out of the appendicular elements examined, the femur and tibia have the highest annual increase in cortical area for the alligators studied, with the femur exceeding that of the tibia. Therefore, alligator femur cortical area increase likely provides an overestimate of alligator tibia cortical area increase. In addition, *Alligator mississippiensis* femoral dimensions are demonstrated to tightly correlate with body length and body mass (Supplementary Figure 3; Fig. 2 and Fig. 3 in Farlow et al. 2005); alligators are well studied and the histological dataset utilized consists of animals of known age, weight, body length, and sex; and alligators are one of the few extant archosaurs approaching the body size of a hadrosaur.

Normalized comparison demonstrates that *Maiasaura* annual cortical increase was highest in the youngest specimens and steadily decreased over ontogeny, but admittedly, the extent to which an ontogenetic transition from bipedal to quadrupedal posture in *Maiasaura* (Dilkes 2001) may affect gait and therefore tibia bone apposition rate is currently unknown. In contrast, even using the femur, alligator cortical growth was much lower, protracted, and more or less constant throughout ontogeny, never approaching the highest rates observed for *Maiasaura*. Because data are normalized, hypotheses for the differences in growth rates observed can then be proposed and tested, such as differences in metabolism, gait, or ecologies.

This normalization method must be applied cautiously, as comparing different skeletal elements from taxa with different limb allometries, gaits, and ecologies can lead to erroneous conclusions about growth (see Zhao et al. 2013; Cullen et al. 2014). Tight correlations with limb element dimensions and body length/mass, as well as maximum appositional growth rates, as noted with the alligator femora, must be demonstrated before being utilized in such normalized comparisons to ensure that the same growth characteristics are being compared. If such conditions are demonstrated, normalized growth comparisons can complement more traditional body mass growth curve modeling. Our evaluation demonstrates two completely different growth histories in related taxa possessing LAGs and provides further evidence that the presence of LAGs is unrelated to metabolism or growth rate, and is likely a plesiomorphic characteristic retained by most, if not all, vertebrate groups (e.g., de Ricqlès et al. 2008).

Physiological Clues in Cortical Features.— Concentric resorption cavity rings (Fig. 5) are observed in the mid cortex of some *Maiasaura* tibiae between 40 cm and 50 cm in length in addition to the typical random scattering of resorption cavities within the innermost cortex. These resorption rings are only found in *Maiasaura* tibiae representing young of the year, and closely resemble structures reported in the humerus of an immature specimen of the sauropod *Alamosaurus* (Woodward and

Lehman 2009). Resorption rings may therefore be a characteristic of young fast growing dinosaur long bones, but only for a brief time. The small sample sizes of most dinosaur histology studies reduce the likelihood of sampling this ontogenetic period, so it is unsurprising this resorption pattern has gone largely unreported in other taxa. Such a concentric arrangement of resorption cavities, rather than the more typical centripetal resorption cavity radiation, may explain how medullary expansion kept pace with the high cortical apposition rates determined here for the very young.

In all *Maiasaura* tibiae with more than two LAGs, a zonal vascular pattern consisting of reticular vascularity followed by laminar or plexiform vascularity appears in the cortical zone representing the third year of life and repeats until approaching skeletal maturity where the zonal spacing makes it difficult to observe (Fig. 4). A similar repeating zonal vascular pattern is described in other dinosaurs (Horner et al. 1999; Hübner 2012; Hedrick et al. 2014) including the hadrosaurid *Edmontosaurus* (Chinsamy et al. 2012). Alaskan specimens of *Edmontosaurus* were hypothesized to exhibit this vascular cyclicity in place of LAGs and in response to annually reduced nutrient access resulting from non migratory behavior and months of polar darkness (Chinsamy et al. 2012). *Maiasaura* vascular cyclicity strongly resembles that of Alaskan *Edmontosaurus* (except that *Maiasaura* also preserves LAGs), but *Maiasaura* inhabited much lower latitudes and would have experienced more temperate conditions (Lorenz and Gavin 1984). The presence of such a vascular pattern therefore provides no evidence of perennial polar residency, and in *Maiasaura* this pattern is consistently only observed after the second LAG.

Rather than a response to non migratory behavior, there is evidence that such a repeating vascular pattern is associated with cyclic hormonal changes. By examining ruminant bone microstructure and recording seasonal hormonal fluctuations, Köhler et al. (2012) found a correlation between increasing levels of growth hormones and increasingly vascularized woven fibered tissue, culminating with the peak of the favorable season. This was

followed by low levels of growth hormones culminating in a growth hiatus of several months during the stressful season, revealed by LAGs in the bone microstructure (Köhler et al. 2012). Therefore the repeating vascular pattern observed in both *Maiasaura* and *Edmontosaurus* was more likely a response to hormonal changes occurring during the favorable season irrespective of elevation or latitude. Another explanation (though not exclusive) for the vascular pattern may be that it indicates a hormonal shift and seasonal reallocation of resources for breeding, egg laying, nest protection, or caring for young, although such life events are often tied to stressful or favorable seasons and may be difficult to separate histologically from environmental reactions. However, if the vascular pattern was solely related to alternating favorable and unfavorable seasons, this pattern should be observed in tissues deposited prior to the third year of growth. The abrupt and permanent switch from largely random vascularity within zones of the youngest *Maiasaura* to a repeating vascular pattern following the second LAG (Fig. 4) in older individuals implies the onset of an annually repeating event affecting growth rate. Based on the *Maiasaura* survivorship curve (Fig. 6), we hypothesized that this taxon attained sexual maturity during the third year of life. Because this vascular pattern appears in the bone tissue during the third year of life, we suggest this pattern is independent evidence of sexual maturity onset at this age. We hypothesize that with increased ontogenetic sampling of polar *Edmontosaurus* a similar trend of ontogenetically delayed cyclic vascularity will almost certainly be revealed.

Linear and Three Dimensional Growth.—A plot of age versus minimum diaphyseal circumference (Fig. 2A) obtained from tibiae with fully traceable LAG circumferences (n = 9) shows individual size variability during ontogeny. On average *Maiasaura* individuals achieved over half (56%, x = 16.6 cm) of their estimated asymptotic tibia circumference of 29.6 cm in their first year, and circumferences varied between 14.2 cm and 18.6 cm (Supplementary Table 2). Circumferences amongst individuals in their third year of life differ by up to 5.2 cm (24% of mean size

at age 2). Growth in tibia circumference begins to plateau between the sixth and eighth year of life, with skeletal maturity occurring in one of these individuals during the eighth year of life.

A high coefficient of determination value (i.e., $R^2 > 0.9$) between tibia length and diaphyseal circumference allows prediction of tibia length and ultimately body mass during each year of growth as represented by LAG circumferences (Supplementary Table 4). Individual ontogenetic variability becomes especially obvious in body mass curves, since variation in linear measurements are essentially cubed in volumetric analyses (Fig. 2). As such, body mass amongst yearlings varies by 296 kg, and by 854 kg at LAG 5. Prior to this study, a single *Maiasaura* body mass curve has been published, constructed upon three data points (Fig. 2 of Erickson et al. 2001). The much larger ontogenetic and longitudinal sample used here allows a synthesis of multiple curves, providing a more accurate portrayal of *Maiasaura* growth and the variability within the species (Fig. 2B). The *Maiasaura* body mass curve published by Erickson et al. (2001) shows a relative stasis in mass increase from age one (160 kg) until age four (172 kg). The authors predicted a maximum growth rate of 1042 kg/year between ages five and six. Although no demonstrably skeletally mature individuals were included in their analysis, Erickson et al. (2001) predicted that *Maiasaura* reached asymptotic body mass at age 7, as was previously calculated by Horner et al. (2000). In contrast, our mean body mass curve suggests a maximum growth rate of 721 kg/yr (95% confidence interval 593–859 kg/yr) occurred during the second year of growth (between LAG 1 and LAG 2) and the mean body mass asymptote of 2337 kg was approached by year eight (Fig. 2B). Individual body mass curves also show a decrease in the rate of annual mass addition after the second LAG (growth of 439–765 kg/yr between LAG 2 and LAG 3, compared to growth of 116–446 kg/yr between LAG 3 and LAG 4), reflected by reduced zone spacing (e.g., Fig. 4A). Lee and Werning (2008) correlated the inflection point on an S shaped curve, occurring between one third and one half asymptotic mass, to the onset of sexual maturity in several dinosaur taxa. Although the inflection point in the *Maiasaura*

mean mass growth curve occurs at 1.44 years of age, one third asymptotic body mass had not yet been attained. Instead, one third of asymptotic body mass is attained just before age 2, and one half of asymptotic body mass is reached soon after age 2 (between LAG 2 and LAG 3; Fig. 2B). The zone between LAG 2 and LAG 3 also coincides with the appearance of a repeating vascular pattern and a temporary mortality increase within the peak performance survivorship plateau, reinforcing our hypothesis that the appearance of an alternating vascular pattern and a temporary increase in mortality rate are independent indicators of sexual maturity.

Conclusions

An ontogenetic sample size of 50 *Maiasaura* tibiae, representing a minimum of 32 individuals, confirmed previously published observations (Varricchio and Horner 1993; Horner et al. 2000), permitted the largest extinct tetrapod population osteohistology synthesis to date, and revealed aspects of *Maiasaura* growth and behavior in unprecedented detail. Our tibia series included individuals less than a year of age up to skeletal maturity and provided not only a complete LAG record for analysis, but also allowed us to observe the individual size and tissue variation present throughout ontogeny. Because of the intraspecific variability present, our study demonstrates that ontogenetic growth studies of extinct tetrapods based on very small datasets must be considered with caution. Strong correlations ($R^2 > 0.9$) between tibia length and diaphyseal circumference, cortical area, and bone wall thickness suggest that such correlations may manifest in other extinct taxa with similarly large ontogenetic sample sets. The corresponding regressions could then be used to construct ontogenetic growth curves for other taxa as was done here for *Maiasaura*. We also demonstrated that *Maiasaura* had avian levels of bone apposition throughout ontogeny, and we incorporate a growth hiatus duration into our apposition rate estimates. Since other extinct tetrapod apposition rates do not incorporate a growth hiatus duration, reanalysis of those datasets should reveal rates

even higher than reported and may necessitate reevaluation of interpretations. By normalizing annual cortical area increase, we directly compared *Maiasaura* growth to an extant archosaur, and showed that although the taxa are related and both possess LAGs, *Maiasaura* grew rapidly early in life and at much higher rates than the slower and protracted rates of *Alligator*. Our study is also the first to satisfy the minimum sample size of 50 as suggested by Steinsaltz and Orzack (2011) for statistically meaningful interpretations of tetrapod survivorship curves, and revealed that survivorship for *Maiasaura* was low during the first year of life and again during the third year of life. Afterward, a survivorship plateau occurred until eight years of age, at the onset of skeletal maturity (mean 8.25 years) and increasing senescence. Many of the observations, interpretations, and quantifications reported herein would not be possible with much smaller sample sizes, especially observing the independent transitions in vascular orientation, survivorship, and body mass accumulation occurring during the third year of life that we hypothesize as indicating sexual maturity. Therefore, the *Maiasaura* dataset thus far acquired demonstrates the potential for large sample population histology analyses, and *Maiasaura* becomes a model organism for use in studies of extinct tetrapod biology.

Acknowledgements

scripts adapted from Cooper et al. (2008), which we modified for this study. *Cervus elaphus* histology image courtesy of M. Köhler. Thanks to J. Schmitt and D. Varricchio for helpful discussion and T. Carr for comments on an earlier manuscript draft. Comments provided by the editor J. Bloch, reviewers S. Werning, D. Evans, and an anonymous reviewer, greatly improved the manuscript. Finally, we would like to thank the more than 30 years of MOR Camp Makela field crews for collecting *Maiasaura* bonebed material.

Literature Cited

Albon, S. D., T. H. Clutton-Brock, and F. E. Guinness. 1987. Early development and population dynamics in red deer. II. Density-independent effects and cohort variation. Journal of Animal Ecology 56:69–81.

Barreto, C. 1997. Dinosaur growth plates and dinosaur bone growth. Pp. 95–100 *in* D. L. Wolberd, E. Stump, and G. D. Rosenberg, eds. Dinofest International: proceedings of a symposium held at Arizona State University. The Academy of Natural Sciences, Tempe, Arizona.

Campione, N., and D. C. Evans. 2012. A universal scaling relationship between body mass and proximal limb bone dimensions in quadrupedal terrestrial tetrapods. BMC Biology 10:1–22.

Castanet, J. 2006. Time recording in bone microstructures of endothermic animals; functional relationships. Comptes Rendus Palevol 5:629–636.

Castanet, J., D. G. Newman, and H. S. Girons. 1988. Skeletochronological data on the growth, age, and population structure of the tuatara, *Sphenodon punctatus*, on Stephens and Lady Alice Islands, New Zealand. Herpetologica 44:25–37.

Castanet, J., H. Francillon-Vieillot, P. J. Meunier, and A. de Ricqlès. 1993. Bone and individual aging. Pp. 245–283 *in* B. K. Hall, ed. Bone CRC Press, London.

Castanet, J., A. Grandin, A. Abourachid, and A. de Ricqlès. 1996. Expression de la dynamique de croissance dans la structure de l'os périostique chez *Anas plathyrhynchos*. Comptes Rendus de l'Academie des Sciences Serie III Sciences de la Vie 319:301–308.

Castanet, J., K. C. Rogers, J. Cubo, and J.-J. Boisard. 2000. Periosteal bone growth rates in extant ratites (ostriche and emu). Implications for assessing growth in dinosaurs. Comptes Rendus de l'Academie des Sciences Serie III Sciences de la Vie 323:543–550.

Castanet, J., S. Croci, F. Aujard, M. Perret, J. Cubo, and E. de Margerie. 2004. Lines of arrested growth in bone and age estimation in a small primate: *Microcebus murinus*. Journal of Zoology, London 263:31–39.

Catchpole, E. A., Y. Fan, B. J. T. Morgan, T. H. Clutton-Brock, and T. Coulson. 2004. Sexual dimorphism, survival and dispersal in red deer. Journal of Agricultural, Biological, and Environmental Statistics 9:1–26.

Chinsamy, A., D. B. Thomas, A. R. Tumarkin-Deratzian, and A. R. Fiorillo. 2012. Hadrosaurs were perennial polar residents. Anat Rec (Hoboken) 295:610–614.

Clutton-Brock, T. H., S. D. Albon, and F. E. Guinness. 1985. Parental investment and sex differences in juvenile mortality in birds and mammals. Nature 313:131.

Cooper, L. N., A. H. Lee, M. L. Taper, and J. R. Horner. 2008. Relative growth rates of predator and prey dinosaurs reflect effects of predation. Proceedings of the Royal Society B-Biological Sciences 275:2609–2615.

Cormack, D. 1987. Ham's Histology. Lippincott Williams and Wilkins, New York.

Cullen, T. M., D. C. Evans, M. J. Ryan, P. J. Currie, and Y. Kobayashi. 2014. Osteohistological variation in growth marks and osteocyte lacunar density in a theropod dinosaur (Coelurosauria: Ornithomimidae). BMC Evolutionary Biology 14:1–14.

de Margerie, E. 2002. Laminar bone as an adaptation to torsional loads in flapping flight. Journal of Anatomy 201:521–526.

de Margerie, E., J. Cubo, and J. Castanet. 2002. Bone typology and growth rate: testing and quantifying 'Amprino's rule' in the mallard (*Anas platyrhynchos*). Comptes Rendus Biologies 325:221–230.

de Margerie, E., J.-P. Robin, D. Verrier, J. Cubo, R. Groscolas, and J. Castanet. 2004. Assessing a relationship between bone microstructure and growth rate: a flourescent labelling study in the king penguin chick (*Aptenodytes patagonicus*). Journal of Experimental Biology 207:869–879.

de Ricqlès, A., K. Padian, F. Knoll, and J. R. Horner. 2008. On the origin of high growth rates in archosaurs and their ancient relatives: complementary histological studies on Triassic archosauriforms and the problem of a "phylogenetic signal" in bone histology. Annales de Paléontologie 94:57–76.

Deevey, E. S. 1947. Life tables for natural populations of animals. The Quarterly Review of Biology 22:283–314.

Dilkes, D. W. 2000. Appendicular myology of the hadrosaurian dinosaur *Maiasaura peeblesorum* from the Late Cretaceous (Campanian) of Montana. Transactions of the Royal Society of Edinburgh: Earth Sciences 90:87–125.

——. 2001. An ontogenetic perspective on locomotion in the Late Cretaceous dinosaur *Maiasaura peeblesorum* (Ornithischia: Hadrosauridae). Canadian Journal of Earth Sciences 38:1205–1227.

Doube, M., M. M. Kłosowski, I. Arganda-Carreras, F. Cordelières, R. P. Dougherty, J. Jackson, B. Schmid, J. R. Hutchinson, and S. J. Shefelbine. 2010. BoneJ: free and extensible bone image analysis in ImageJ. Bone 47:1076–1079.

Erickson, G. M. 1996. Daily deposition of dentine in juvenile *Alligator* and assessment of tooth replacement using line counts. Journal of Morphology 228:189–194.

——. 2005. Assessing dinosaur growth patterns: a microscopic revolution. TRENDS in Ecology and Evolution 20:677–684.

Erickson, G. M., and T. A. Tumanova. 2000. Growth curve of *Psittacosaurus mongoliensis* Osborn (Ceratopsia: Psittacosauridae) inferred from long bone histology. Zoological Journal of the Linnean Society 130:551–566.

Erickson, G. M., K. R. Rogers, and S. A. Yerby. 2001. Dinosaurian growth patterns and rapid avian growth rates. Nature 412:429–432.

Erickson, G. M., P. J. Currie, B. D. Inouye, and A. A. Winn. 2006. Tyrannosaur life tables: an example of nonavian dinosaur population biology. Science 313:213–217.

——. 2010. A revised life table and survivorship curve for *Albertosaurus sarcophagus* based on the Dry Island mass death assemblage. Canadian Journal of Earth Sciences 47:1269–1275.

Erickson, G. M., P. J. Makovicky, B. D. Inouye, C. F. Zhou, and K. Q. Gao. 2009. A life table for Psittacosaurus lujiatunensis: initial insights into ornithischian dinosaur population biology. Anat Rec (Hoboken) 292:1514–1521.

Farlow, J. O., and A. Britton. 2000. Size and body proportions in *Alligator mississippiensis*: implications for archosaurian ichnology. Paleontological Society of Korea Special Publication 4:189–206.

Farlow, J. O., G. R. Hurlburt, R. M. Elsey, A. R. C. Britton, and W. Langston Jr. 2005. Femoral dimensions and body size of *Alligator mississippiensis*: estimating the size of extinct mesoeucrocodylians. Journal of Vertebrate Paleontology 25:354–369.

Farmer, C. G., and K. Sanders. 2010. Unidirectional airflow in the lungs of alligators. Science 327:338–340.

Francillon-Vieillot, H., V. de Buffrenil, J. Castanet, J. Geraudie, F. J. Meunier, J. Y. Sire, L. Zylberberg, and A. de Ricqlès. 1990. Microstructure and mineralization of vertebrate skeletal tissues. Pp. 471–548 in J. G. Carter, ed. Skeletal Biomineralization: Patterns, Processes and Evolutionary Trends, Volume 1. Van Nostrand Reinhold, New York.

Games, I. 1990. Growth curves for the Nile crocodile as estimated by skeletochronology. Pp. 111–121. Proceedings of the 10th Working Meeting of the Crocodile Specialist Group. Species Survival Commission of the International Union for the Conservation of Nature and Natural Resources, Gainesville, Florida.

Gates, T. A., J. R. Horner, R. R. Hanna, and C. R. Nelson. 2011. New unadorned hadrosaurine hadrosaurid (Dinosauria, Ornithopoda) from the Campanian of North America. Journal of Vertebrate Paleontology 31:798–811.

Hedrick, B. P., A. Tumarkin-Deratzian, and P. Dodson. 2014. Bone microstructure and relative age of the holotype specimen of the diplodocid sauropod Suuwassea emilieae. Acta Palaeontologica Polonica 59:295–304.

Horner, J. R. 1982. Evidence of colonial nesting and 'site fidelity' among ornithischian dinosaurs. Nature 297:675–676.

——. 1983. Cranial osteology and morphology of the type specimen of Maiasaura peeblesorum (Ornithischia: Hadrosauridae), with discussion of its phylogenetic position. Journal of Vertebrate Paleontology 3:29–38.

——. 1992. Cranial Morphology of Prosaurolophus (Ornithischia: Hadrosauridae): With Descriptions of Two New Hadrosaurid Species and an Evaluation of Hadrosaurid Phylogenetic Relationships. Museum of the Rockies Occasional Paper 2:1–120.

——. 1999. Egg clutches and embryos of two hadrosaurian dinosaurs. Journal of Vertebrate Paleontology 19:607–611.

Horner, J. R., and R. Makela. 1979. Nest of juveniles provides evidence of family structure among dinosaurs. Nature 282:296–298.

Horner, J. R., A. de Ricqlès, and K. Padian. 1999. Variation in dinosaur skeletochronology indicators: implications for age assessment and physiology. Paleobiology 25:295–304.

——. 2000. Long bone histology of the hadrosaurid dinosaur Maiasaura peeblesorum: growth dynamics and physiology based on an ontogenetic series of skeletal elements. Journal of Vertebrate Paleontology 20:115–129.

Horner, J. R., K. Padian, and A. de Ricqlès. 2001. Comparative osteohistology of some embryonic and perinatal archosaurs: developmental and behavioral implications for dinosaurs. Paleobiology 27:39–58.

Horner, J. R., M. B. Goodwin, and N. Myhrvold. 2011. Dinosaur census reveals abundant Tyrannosaurus and rare ontogenetic stages in the Upper Cretaceous Hell Creek Formation (Maastrichtian), Montana, USA. Plos One 6:e16574. doi: 10.1371/journal.pone.0016574.

Hübner, T. R. 2012. Bone histology in Dysalotosaurus lettowvorbecki (Ornithischia: Iguanodontia) - variation, growth, and implications. Plos One 7:e22958. doi: 10.1371/journal.pone.0029958.

Joanen, T., and L. McNease. 1987. Alligator farming research in Louisiana, USA. Pp. 329–340 in J. W. Grahame, S. Webb, C. Manolis, and P. J. Whitehead, eds. Wildlife Management: Crocodiles and Alligators. Surrey Beatty and Sons, Chipping Norton, NSW, Australia.

Jones, O. R., J. M. Gaillard, S. Tuljapurkar, J. S. Alho, K. B. Armitage, P. H. Becker, P. Bize, J. Brommer, A. Charmantier, M. Charpentier, T. Clutton-Brock, F. S. Dobson, M. Festa-Bianchet, L. Gustafsson, H. Jensen, C. G. Jones, B. G. Lillandt, R. McCleery, J. Merila, P. Neuhaus, M. A. Nicoll, K. Norris, M. K. Oli, J. Pemberton, H. Pietiainen, T. H. Ringsby, A. Roulin, B. E. Saether, J. M. Setchell, B. C. Sheldon, P. M. Thompson, H. Weimerskirch, E. Jean Wickings, and T. Coulson. 2008. Senescence rates are determined by ranking on the fast-slow life-history continuum. Ecology Letters 11:664–673.

Kilbourne, B. M., and P. J. Makovicky. 2010. Limb bone allometry during postnatal ontogeny in non-avian dinosaurs. Journal of Anatomy 217:135–152.

Klein, N., T. Scheyer, and T. Tütken. 2009. Skeletochronology and isotopic analysis of a captive individual of Alligator mississippiensis Daudin, 1802. Fossil Record 12:121–131.

Köhler, M., N. Marin-Moratalla, X. Jordana, and R. Aanes. 2012. Seasonal bone growth and physiology in endotherms shed light on dinosaur physiology. Nature 487:358–361.

Lamm, E. T. 2013. Chapter 4: Preparation and Sectioning of Specimens. Pp. 55–160 in K. Padian, and E. T. Lamm, eds. Bone Histology of Fossil Tetrapods: Advancing Methods, Analysis, and Interpretation. University of California Press, Berkeley.

Lance, V. A. 1989. Reproductive cycle of the American alligator. American Zoologist 29:999–1018.

Lee, A., and P. O'Connor. 2013. Bone histology confirms determinate growth and small body size in the noasaurid theropod Masiakasaurus knopfleri. Journal of Vertebrate Paleontology 33:865–876.

Lee, A. H., and S. Werning. 2008. Sexual maturity in growing dinosaurs does not fit reptilian growth models. Proceedings of the National Academy of Sciences of the United States of America 105:582–587.

Lee, A. H., A. Huttenlocker, K. Padian, and H. N. Woodward. 2013. Chapter 8: Analysis of Growth Rates. Pp. 217–251 in K. Padian, and E. T. Lamm, eds. Bone Histology of Fossil Tetrapods: Advancing Methods, Analysis, and Interpretation. University of California Press, Berkeley.

Lorenz, J. C., and W. Gavin. 1984. Geology of the Two Medicine Formation and the sedimentology of a dinosaur nesting ground. Pp. 175–187. Field Conference Northwestern Montana. Montana Geological Society.

Montes, L., J. Castanet, and J. Cubo. 2010. Relationship between bone growth rate and bone tissue organization in amniotes: first test of Amprino's rule in a phylogenetic context. Animal Biology 60:25–41.

Myhrvold, N. P. 2013. Revisiting the estimation of dinosaur growth rates. Plos One 8:e81917. doi:10.1371/journal.pone.0081917.

Nussey, D. H., A. J. Wilson, A. Morris, J. Pemberton, T. H. Clutton-Brock, and L. E. B. Kruuk. 2008. Testing for genetic trade-offs between early- and late-life reproduction in a wild red deer population. Proceedings of the Royal Society B 275:745–750.

Nussey, D. H., L. E. B. Kruuk, A. Morris, M. N. Clements, J. M. Pemberton, and T. H. Clutton-Brock. 2009. Iner- and intrasexual variation in aging patterns across reproductive traits in a wild red deer population. The American Naturalist 174:342–357.

Peabody, F. E. 1961. Annual growth zones in living and fossil vertebrates. Journal of Morphology 108:11–62.

Pearl, R., and J. R. Miner. 1935. Experimental studies on the duration of life. XIV. The comparative mortality of certain lower organisms. The Quarterly Review of Biology 10:60–79.

R Development Core Team 2010. R: A language and environment for statistical computing. R Foundation for Statistical Computing, Vienna, Austria. http://www.R-project.org.

Rasband, W. S. 1997–2014. U. S. National Institutes of Health, Bethesda, Maryland, USA. http://imagej.nih.gov/ij/.

Richards, F. J. 1959. A flexible growth function for empirical use. Journal of Experimental Botany 10:290–300.

Rogers, R. R. 1990. Taphonomy of three dinosaur bone beds in the Upper Cretaceous Two Medicine Formation of northwestern Montana: evidence for drought-related mortality. Palaios 5:394–413.

——. 1993. Systematic patterns of time-averaging in the terrestrial vertebrate record. In S. M. Kidwell, and A. K. Behrensmeyer, eds. Taphonomic Approaches to Time Resolution in Fossil Assemblages. Paleontological Society Short Courses in Paleontology 6.

Schmitt, J. G., F. D. Jackson, and R. R. Hanna. 2014. Debris flow origin of an unusual late Cretaceous hadrosaur bonebed in the Two Medicine Formation of western Montana. Pp. 486–501 *in* D. Eberth, and D. Evans, eds. Hadrosaurs. Indiana Press, Bloomington.

Schweitzer, M. H., J. L. Wittmeyer, and J. R. Horner. 2005. Gender-specific reproductive tissue in ratites and *Tyrannosaurus rex*. Science 308:1456–1460.

Schweitzer, M. H., R. M. Elsey, C. G. Dacke, J. R. Horner, and E. T. Lamm. 2007. Do egg-laying crocodilian (*Alligator mississippiensis*) archosaurs form medullary bone? Bone 40:1152–1158.

Starck, J. M., and A. Chinsamy. 2002. Bone microstructure and developmental plasticity in birds and other dinosaurs. Journal of Morphology 254:232–246.

Steinsaltz, D., and S. H. Orzack. 2011. Statistical methods for paleodemography on fossil assemblages having small numbers of specimens: an investigation of dinosaur survival rates. Paleobiology 37:113–125.

Trueman, C. N. 1999. Rare earth element geochemistry and taphonomy of terrestrial vertebrate assemblages. Palaios 14: 555–568.

Trueman, C. N., and M. J. Benton. 1997. A geochemical method to trace the taphonomic history of reworked bones in sedimentary settings. Geology 25:263–266.

Tumarkin-Deratzian, A. R. 2007. Fibrolamellar bone in wild adult *Alligator mississippiensis*. Journal of Herpetology 41:341–345.

Tumarkin-Deratzian, A. R., D. R. Vann, and P. Dodson. 2007. Growth and textural ageing in long bones of the American alligator *Alligator mississippiensis* (Crocodylia: Alligatoridae). Zoological Journal of the Linnean Society 150:1–39.

Varricchio, D. J., and J. R. Horner. 1993. Hadrosaurid and lambeosaurid bone beds from the Upper Cretaceous Two Medicine Formation of Montana: taphonomic and biologic implications. Canadian Journal of Earth Sciences 30:997–1006.

Varricchio, D. J., C. Koeberl, R. F. Raven, W. Wolbach, W. C. Elsik, and D. P. Miggins. 2010. Tracing the Manson impact event across the Western Interior Cretaceous Seaway. Pp. 269–299 *in* W. U. Reimold, and R. L. Gibson, eds. Proceedings of the Conference on Large Meteorite Impacts and Planetary Evolution IV. The Geological Society of America.

Voorhies, M. R. 1969. Taphonomy and population dynamics of an Early Pliocine vertebrate fauna, Knox County, Nebraska. Contributions to Geology Special Paper 8, 1–69.

Wilkinson, P. M., and W. E. Rhodes. 1997. Growth rates of American alligators in coastal South Carolina. Journal of Wildlife Management 61:397–402.

Woodward, H. N., and T. M. Lehman. 2009. Bone histology and microanatomy of *Alamosaurus sanjuanensis* (Sauropoda: Titanosauria) from the Maastrichtian of Big Bend National Park, Texas. Journal of Vertebrate Paleontology 29:807–821.

Woodward, H. N., J. R. Horner, and J. O. Farlow. 2011. Osteohistological evidence for determinate growth in the American alligator. Journal of Herpetology 45:339–342.

——. 2014. Quantification of intraskeletal histovariability in *Alligator mississippiensis* and implications for vertebrate osteohistology. PeerJ 2:e422. doi: 10.7717/peerj.422.

Zhao, Q., M. J. Benton, C. Sullivan, P. M. Sander, and X. Xu. 2013. Histology and postural change during the growth of the ceratopsian dinosaur *Psittacosaurus lujiatunensis*. Nature Communications 4:2079. doi: 10.1038/ncomms3079.